AD-782 940

DEVELOPMENT OF METHODS TO DETERMINE THE HUGONIOT EQUATION-OF-STATE OF CONCRETE

Anthony A. Bombich

Army Engineer Waterways Experiment Station
Vicksburg, Mississippi

June 1974

Unclassified
Security Classification

AD-782940

DOCUMENT CONTROL DATA - R & D

(Security classification of title, body of abstract and indexing annotation must be entered when the overall report is classified)

1 ORIGINATING ACTIVITY (Corporate author)
U. S. Army Engineer Waterways Experiment Station
Vicksburg, Mississippi

2a. REPORT SECURITY CLASSIFICATION
Unclassified

2b. GROUP

3 REPORT TITLE
DEVELOPMENT OF METHODS TO DETERMINE THE HUGONIOT EQUATION-OF-STATE OF CONCRETE

4 DESCRIPTIVE NOTES (Type of report and inclusive dates)
Final report

5. AUTHOR(S) (First name, middle initial, last name)
Anthony A. Bombich

6 REPORT DATE	7a. TOTAL NO. OF PAGES	7b. NO. OF REFS
June 1974	85	34

8a CONTRACT OR GRANT NO.	9a. ORIGINATOR'S REPORT NUMBER(S)
b. PROJECT NO 4A061101A91D	Miscellaneous Paper C-74-10
c. Task 02	9b. OTHER REPORT NO(S) (Any other numbers that may be assigned this report)
d.	

10. DISTRIBUTION STATEMENT
Approved for public release; distribution unlimited.

11. SUPPLEMENTARY NOTES	12. SPONSORING MILITARY ACTIVITY
	Assistant Secretary of the Army (R&D), Department of the Army Washington, D. C.

13 ABSTRACT

Methods used to determine the Hugoniot equation-of-state were experimentally evaluated for structural concrete having 3/4-in. (prototype) and 1/8-in. (modeled) aggregate sizes. Shock wave simulations were conducted using a two-dimensional shock-wave propagation computer code. Results showed that Hugoniot tests could be conducted on the prototype concrete within acceptable tolerances of experimental error. Results also showed that the Hugoniot equation-of-state of the prototype concrete can be matched with a modeled concrete mixture. Shock propagation simulations of a computer modeled prototype concrete were found to closely reproduce the Hugoniot of the prototype. In-material stress and particle velocity gage methods and Lagrangian data analysis techniques were used extensively in this work. The experimental methods and analysis techniques are discussed in detail. Experimental and simulated shock profiles and material response curves are also presented and discussed in this report. Recommendations pertaining to important experimental design criteria as well as for further study are also included.

DD FORM 1 NOV 68 1473 REPLACES DD FORM 1473, 1 JAN 64, WHICH IS OBSOLETE FOR ARMY USE.

Unclassified
Security Classification

Unclassified

Security Classification

KEY WORDS	LINK A		LINK B		LINK C	
	ROLE	WT	ROLE	WT	ROLE	WT
Computerized simulation						
Concrete structures						
Concretes						
Dynamic loads						
Hugoniot equations of state						
Shock waves						

Unclassified

Security Classification

THE CONTENTS OF THIS REPORT ARE NOT TO BE USED FOR ADVERTISING, PUBLICATION, OR PROMOTIONAL PURPOSES. CITATION OF TRADE NAMES DOES NOT CONSTITUTE AN OFFICIAL ENDORSEMENT OR APPROVAL OF THE USE OF SUCH COMMERCIAL PRODUCTS.

FOREWORD

The project entitled "Development of Methods to Determine the Hugoniot Equation-of-State of Concrete" was funded by Department of the Army Project 4A 061101A91D, Task 02, "In-House Laboratory Independent Research Program," sponsored by the Assistant Secretary of the Army (R&D).

The work was conducted in the Concrete Laboratory of the U. S. Army Engineer Waterways Experiment Station (WES) under the direction of Messrs. Bryant Mather, R. V. Tye, Jr., Leonard Pepper, and B. R. Sullivan during the period November 1971 to June 1974. Mr. A. A. Bombich was the project leader and prepared this report.

Directors of the WES during this period were BG Ernest D. Peixotto, CE, and COL G. H. Hilt, CE. Technical Director was Mr. F. R. Brown.

CONTENTS

CONTENTS

CONTENTS

CONVERSION FACTORS, U. S. CUSTOMARY TO METRIC (SI) UNITS OF MEASUREMENT

U. S. customary units of measurement used in this report can be converted to metric (SI) units as follows:

Multiply	By	To Obtain
inches	2.54	centimetres
feet	0.3048	metres
feet per second	0.3048	metres per second
bars	100,000	pascals
kilobars	100,000	kilopascals
pounds	4.53592/	kilograms
94-lb bags per cubic yard	55.7679806	kilograms per cubic metre
cubic feet	0.02813168	cubic metres
pounds per square inch	6894.757	pascals

SUMMARY

Methods used to determine the Hugoniot equation-of-state were experimentally evaluated for structural concrete having 3/4-in. (prototype) and 1/8-in. (modeled) aggregate sizes. Shock wave simulations were conducted using a two-dimensional shock-wave propagation computer code. Results showed that Hugoniot tests could be conducted on the prototype concrete within acceptable tolerances of experimental error. Results also showed that the Hugoniot equation-of-state of the prototype concrete can be matched with a modeled concrete mixture. Shock propagation simulations of a computer modeled prototype concrete were found to closely reproduce the Hugoniot of the prototype. In-material stress and particle velocity gage methods and Lagrangian data analysis techniques were used extensively in this work. The experimental methods and analysis techniques are discussed in detail. Experimental and simulated shock profiles and material response curves are also presented and discussed in this report. Recommendations pertaining to important experimental design criteria as well as for further study are also included.

DEVELOPMENT OF METHODS TO DETERMINE THE HUGONIOT EQUATION-OF-STATE OF CONCRETE

PART I: INTRODUCTION

Background

1. For defense-oriented structures to survive shock-loading environments consideration must be given to their structural response. The shock loading on a structure may be the result of nuclear blasts, conventional explosions, or high velocity impact. In recent years elaborate computer codes have been used to evaluate the effects of shock loadings on such structures. Necessary input to these codes is the shock-loading physical properties of the structural materials used. This is the case for calculations which predict and verify prototype response as well as the response of modeled structures experimentally subjected to shock loading. Concrete is a primary construction material and its shock response properties have therefore become increasingly important. Determining these properties is complicated by the composition of concrete.

2. The basic representation of a material's shock properties is the Hugoniot equation-of-state (EOS), which is defined as the locus of final state points achieved by shock loading or through a shock transition. Experiments to determine the EOS of materials involve subjecting prepared samples to a plane shock provided by either direct contact explosives or explosively or gun driven flat plate impact. The varied

measurement techniques used to provide data from the experiment are most accurate when homogeneous and fine-grained materials are tested. As the particle sizes of the specimen material become larger, changes in the measurement technique must be made to ensure accuracy. However, there are definite limits to these changes governed by the laboratory facilities, the method(s) of measurement, and the shock wave stability of the materials. Hence, materials composed of grains larger than 1/8 in. have been avoided if possible, especially if the composites which comprise the material differ greatly in physical properties. An alternative to testing such unsatisfactory material has been through reconstitution of the material into composition of finer grain sizes. This method has proved questionable for rocks and soils due to the inability to duplicate specifically a product of nature. There is no check short of comparative EOS testing to be assured that the resulting material will possess the same EOS as the original. However, if the EOS of the original must be determined to validate the reconstitution, then reconstitution in most cases is unnecessary.

3. Man-made materials such as concrete can be reconstituted to match more closely the properties of the original material. The problem remains. Has the EOS been duplicated or matched? Even though modeled aggregate concretes have been developed and used as accepted duplicates of the prototype sized aggregate mixtures, problems and questions persist as to the matching of shock response. Those which immediately arise are: (a) Fine aggregate concretes inherently possess a higher porosity than large aggregate concretes--a factor strongly affecting low stress

compressibility, (b) How does the increase in cement paste-aggregate interface area or number of interfaces in small aggregate concrete affect its shock propagation properties when compared to that of the prototype mixture? (c) There exists a substantial lack of knowledge pertaining to the relation of static properties to shock properties when dimensional composition of the material is changed. Thus far, these problems and questions have not been resolved, or worse, have been ignored.

Purpose and Scope

4. The purpose of this study was to determine the feasibility of EOS testing of larger aggregate (> 1/8-in.) concretes and to examine the relationship between prototype and modeled mixtures as a reference for future work. This was to be accomplished by experimental tests supplemented by data provided by computer simulations of wave propagation through a composite material model. The result of the work is to conclude, under present limitations of experimental test criteria, whether data from EOS tests of large aggregate concrete fall within an acceptable range of accuracy. Other goals were to determine the methods of measurement and sample configurations or both that may be employed to attain this end and to determine whether a concrete mixture modeled with small aggregate is an EOS match for the prototype as intended.

PART II: CONCRETE AND EQUATION-OF-STATE TESTING

5. Concrete has been defined as: "A composite material which consists essentially of a binding medium within which are embedded particles or fragments of aggregate."[1] Specifically, concrete is made up of coarse and fine aggregate, hydrated cement, unhydrated cement, capillary pores, free water, and air voids. By varying basic materials, the proportions of the materials, and the procedures of preparation, many concrete mixtures are possible with a variety of physical and material properties.

6. Because the EOS of any material is based upon the physical and material composition, it is then obvious that a variable material such as concrete can possess EOS over a wide range of values. Concrete intended for specific purposes, such as structural concrete intended for shock resistance, would not vary as much in EOS properties because of the more narrow range in physical and material properties. However, the expected variation in EOS for structural concrete has not been established since an insufficient number of these concrete mixtures have been examined for EOS properties and those examined were limited basically to small-sized aggregates.

7. It is necessary in equation-of-state experiments as in other laboratory testing that the specimen size and method of measurement be determined by the maximum particle sizes within the tested material. The objective in a proper testing technique is to be assured that the results

of a test are not a function of the internal physical configuration of the components and that external specimen dimensions do not effect a change in results.

8. Many "rules of thumb" have been developed over the years which limit dimension relationships in test specimens. Based upon data produced in this study it will be shown for purposes of practicality in EOS testing of larger aggregate concretes that certain of these relationships can be modified.

PART III: HUGONIOT EQUATION-OF-STATE-- THEORETICAL AND EXPERIMENTAL CONSIDERATIONS

9. This section reviews the basic theory of shock waves in solids, describes measurement techniques that have been used to collect experimental data, and describes the experimental methods used to generate plane shocks in test specimens.

Theoretical Background

10. The Rankine-Hugoniot Curve (Hugoniot) is the locus of final states that can be reached from an initial state by a shock transition. The Hugoniot curve, described by the Hugoniot equation-of-state, can be shown in the stress-volume, stress-particle velocity, or shock velocity-particle velocity planes. For single, steady plane-wave shocks the values of the state variables, pressure or stress (σ), and specific volume (V), on either side of the shock, as well as the kinetic variables, shock propagation velocity (U) and particle velocity (u), are related by the Rankine-Hugoniot equation:[2,3]

$$\frac{V_1}{V_o} = \frac{U - u_1}{U - u_o} \quad \text{, conservation of mass,} \tag{1}$$

$$\sigma_1 - \sigma_o = \frac{(U - u_o)(u_1 - u_o)}{V_o} \quad \text{, conservation of momentum.} \tag{2}$$

The subscript o refers to states in front of the shock and 1 refers to states behind the shock. In the case of a shock with a two-wave structure the equations are applied twice. A two-wave structure may be caused by yielding at the Hugoniot elastic limit (HEL) or because of a shock-induced phase change. Figures 1 and 2 depict single and double shocks and hypothetical Hugoniot.

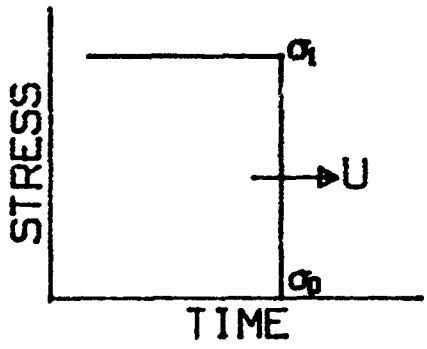

Figure 1A.

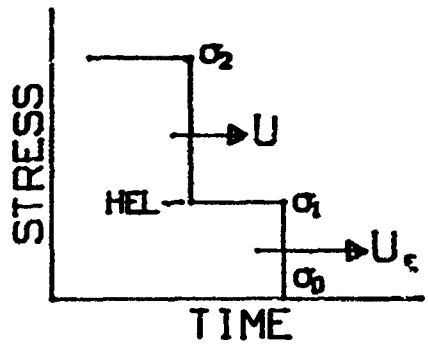

Figure 1B.

Figure 1. Single and double shock wave structure

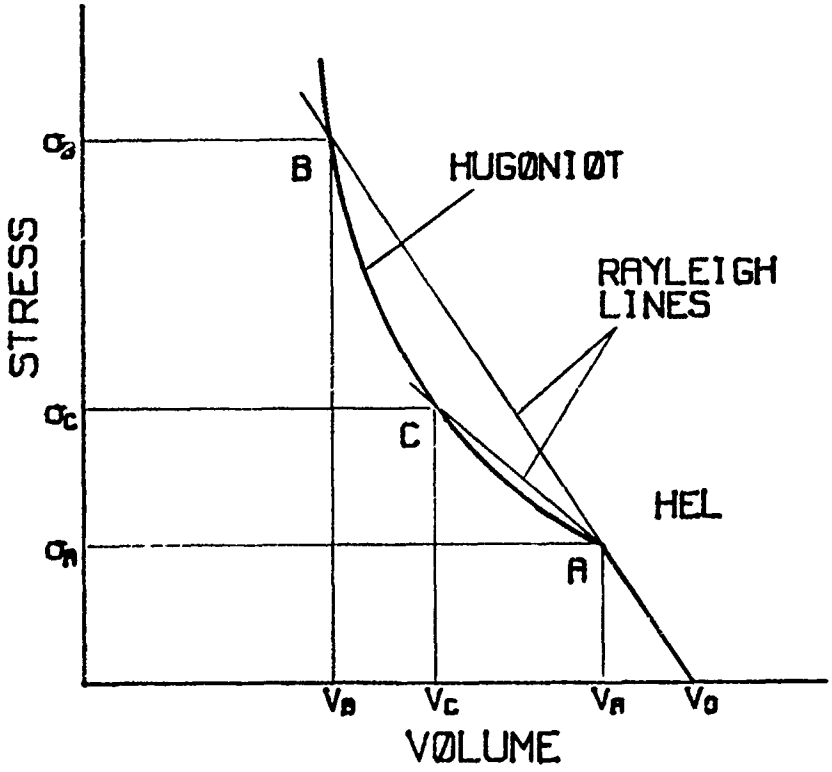

Figure 2. Hypothetical Hugoniot in stress-volume plane

11. A single shock as in Figure 1A can exist at stresses less than σ_A and greater than σ_B in Figure 2. Point B is defined by the intersection of the Hugoniot and a Rayleigh line, or shock chord drawn between shocked states, passing through A and V_o. Shock stresses between σ_A and σ_B are unstable and will separate into two shock fronts propagating at different velocities as shown in Figure 1B. The leading shock has an amplitude $\sigma = \sigma_1 = \sigma_A$ (HEL), is called an elastic precursor, and travels at very nearly the longitudinal elastic sound velocity, U_E. The second front is called the deformational shock and moves at a lower velocity, U. In order to determine the states behind the second wave the states behind the first wave must first be calculated using Equations 1 and 2 where the subscript o is ambient laboratory conditions and subscript 1 is the HEL at A. A second calculation is then performed with the subscripts in Equations 1 and 2 incremented by one so that subscript 1 becomes the initial state at A and subscript 2 is the final state represented by C in Figure 2. If the material is subjected to a shock at other stress levels within the unstable zone the second or final state will lie on the Hugoniot between A and B achieved along other shock chords.

12. If σ_2 is greater than σ_B the deformational shock will overdrive the elastic wave and again become stable so that the elastic wave does not form, even momentarily. This condition exists when the shock stress is greater than σ_B of Figure 2 and the velocity of propagation, U, is greater than longitudinal elastic sound velocity, U_E. Stresses above σ_B are hydrodynamic pressures since residual material strength effects may be neglected. This region is termed hydrodynamic.

13. Most solids will possess a Hugoniot as shown in Figure 2; however, the HEL and the onset of the hydrodynamic state will vary considerably with the material. The HEL for some materials may be extremely low as to appear nonexistent. By comparison the HEL for many materials such as granite-like rocks may be greater than 100 kilobars. The states A and B exist over a wide range depending on the particular material. Fluids possess no material rigidity, have no HEL, and thus are hydrodynamic and are stable except for phase changes.

14. Many materials at stress levels below B in Figure 2 do not exhibit the ideally step-shaped shock fronts shown in Figure 1. The shock steps, especially that of the elastic precursor, have been observed to be rounded and the transition from step to step is ramp-like. Or the precursor may be completely ramp-like and no well-resolved precursor is seen. This type of shock front and the resulting hypothetical Hugoniot is shown in Figure 3.

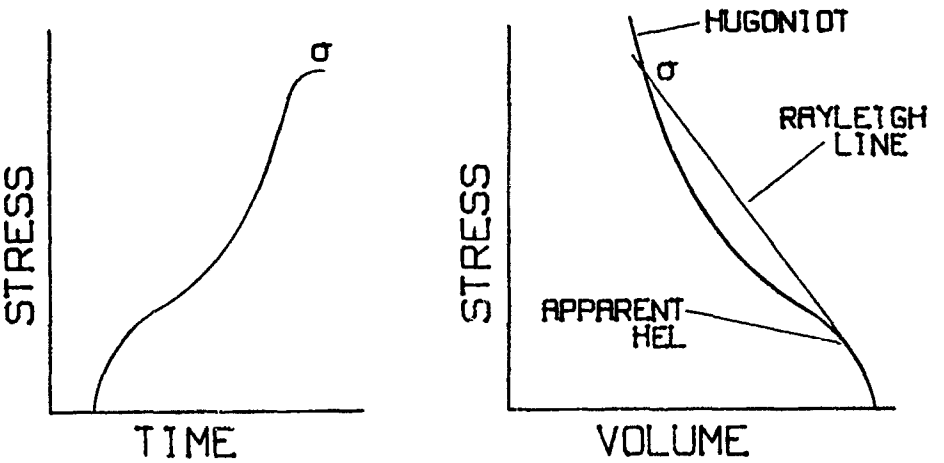

Figure 3. Ramped shock wave structure and resulting stress-volume Hugoniot

The type of material behavior shown in Figure 3 has served to advance measurement and calculational methods through the use of multiple in-material gages. Propagation velocities can be determined between gages at increments of stress or particle velocity. Equations 1 and 2 or forms thereof are then used to calculate shock states in a manner similar to that described earlier for double wave shock fronts, but at smaller increments. These calculations result in the hypothetical Hugoniot shown in Figure 3B where the lower "elastic" portion is curved. An apparent HEL can be determined although this state will not be as well defined as seen earlier for an ideal double shock.

15. A concept called stress relaxation[4] has been observed that applies to materials undergoing a shock transition in the unstable shock region. This phenomenon is manifested by a decay in amplitude of the elastic precursor in an elastoplastic solid during the early stages of shock propagation. This phenomenon occurs very soon after impact and is associated with the finite time required for plastic yielding to occur. The result, in observing the shock wave, is a condition where the precursor is equilibrating to a steady state condition. This phenomenon may be a contributing factor in the development of poorly-defined precursor waves especially in composite materials where the constituent materials differ in time dependent yield properties.

Plane Shock Generation

16. Several methods have been used to generate plane shocks in test specimens. Each method has some limitations; consequently, the

system of shock generation to be used is usually based upon the shock stresses desired, specimen size, or composition, and/or combinations of factors unique to the particular test. This section describes generally several commonly used shock generation methods.

Direct Contact Method

17. The assembly shown in Figure 4 serves to input a plane shock wave into the driver plate at shock pressures dependent upon the type of high explosives (HE) driver and the driver plate material. All of the components of the system, including the explosives, are machined to close tolerances for purposes of preserving planarity and uniformity of shock pressure. The stability and duration[3] of the shock wave can be enhanced through increased explosives-specimen thickness ratio and the use of an air or vacuum gap between the HE driver and driver plate.

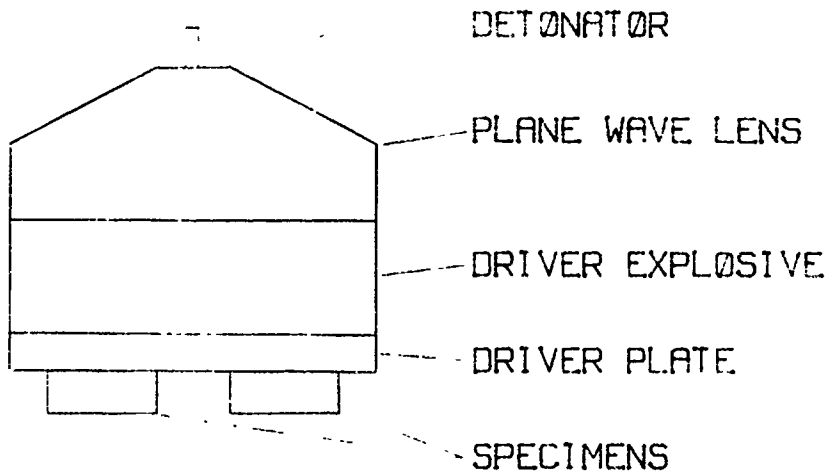

Figure 4. Direct contact high explosives system

The increased explosives thickness increases the pulse duration and the gap serves to reduce peak pressures at the detonation front causing a longer and more uniform peak pressure-time (flat-topped) shock pulse. These explosives systems have been used at diameters up to 12 in.; however, the 8-in. and 6-in. diameter systems are most common. The effective plane wave area for specimen size purposes is approximately 1-2 in. less than the diameter of the explosives system.

18. The driver plate transmits the shock to the specimen. The driver plate must have a well known stress-particle velocity Hugoniot and release curve (often called a cross curve). Several materials such as aluminum, brass, other metals, and plastics have been used. The dynamic variables, shock velocity U, and the free surface velocity ufs, in the specimen, or the free surface velocity of the driver plate are measured. The impedance match method (to be described later) is then used to determine the Hugoniot states in the specimen. Peak pressure possible with this system is about 400 kilobars.

Explosive Flyer Plate System

19. The explosive flyer plate method[3,5] is used to produce shock states beyond that possible with the direct contact method. An illustration of this system is shown in Figure 5. The system is similar to the direct contact system except that the high explosive detonation gases accelerate a flyer plate across a gap. The flyer plate impacts the driver plate inducing shock pressures greater than that possible with the direct contact system. The shock profile is flat-topped over a time proportional to the

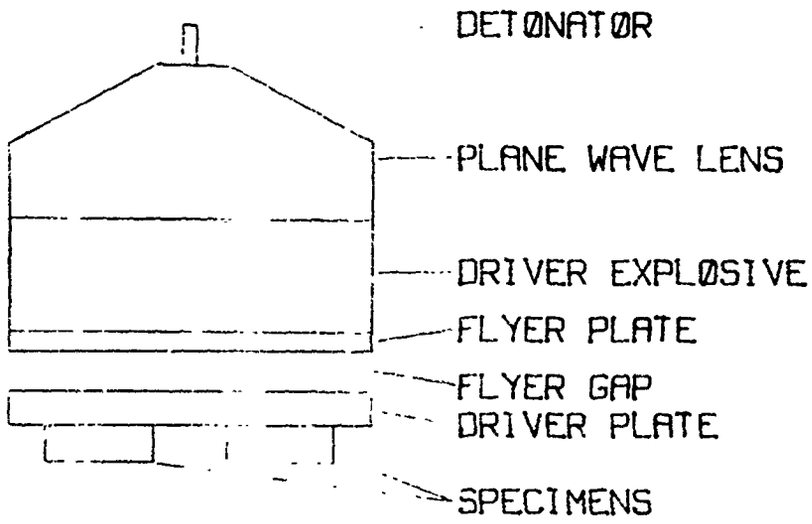

Figure 5. Flyer plate high explosives system

flyer plate thickness. Driver plate pressures between 200 and 900 kilobars are possible with the flyer-plate system through various conformations of flyer and driver materials, gap distances, and explosive drivers. Measurement and data reduction techniques that can be used are the same as are available in the direct contact method.

Gun Systems

20. In all gun systems flat-faced projectiles of various configuration are impacted upon the test specimen to produce the shock

desired in the specimen. Three basic types of guns[6,7,8] are being used in various laboratories in EOS testing. These types and the maximum impact velocities of each are:

Compressed gas	> 0.8 km/sec (2500 ft/sec)
Powder	> 2.6 km/sec (8000 ft/sec)
Powder-light gas	> 8.5 km/sec (25,000 ft/sec)

Compressed-gas guns use compressed nitrogen, helium, and sometimes compressed air to drive the projectile. Powder guns use the expanding gas products produced by detonating gunpowder to propel the projectile. Powder-light-gas guns are two stage guns in which gunpowder is used to propel a piston into a compressed-gas reservoir. This causes the gas to become highly compressed, ultimately propelling projectiles to very high velocities.

21. Most EOS tests are accomplished with gas and powder guns. However, regardless of the type of gun the basic projectile and target configurations are readily modifiable to accomplish the particular experimental goals. Projectile bodies normally are lightweight material with impactor disks bonded to them. The shock stresses can be varied by using impactor plates of different materials and by varying the impact velocity. The shock pulse length can be varied by employing various thicknesses of the impactor disk. In cases where maximum pulse width is desired the entire projectile may be fabricated of the impactor material. Measures are taken to ensure plane impact through careful machining of the projectile and by carefully aligning the impact face of the target specimen. Gun systems allow a greater amount of flexibility in test design and measurement

methods, the only limitations being a fixed bore diameter, usually less than 102 mm (4 in.), and impact velocity limits. Most of the recent developments in gaging techniques and data-reduction methods have developed from the laboratory controlled environment of gun systems.

Measurement Techniques

22. A variety of measurement techniques to obtain EOS data have been used. Many have been abandoned as the measurement state of the art has advanced. This section describes the methods most widely used at the present time and the advantages and disadvantages of each.

Time of arrival pins/ impedance match method[9,10]

23. Time of arrival (TOA) pins are used to measure shock arrival. Under conditions of stable, single wave shocks, TOA pins may be used to measure shock transit times, hence, shock propagation velocity through specimens, and can be used to measure free surface or impact velocity. In cases of stable, single wave shocks TOA pins in conjunction with the impedance match data reduction method will provide complete Hugoniot state information.

24. The impedance match method in its simplest form is briefly described below. A graphical representation is illustrated in Figure 6.

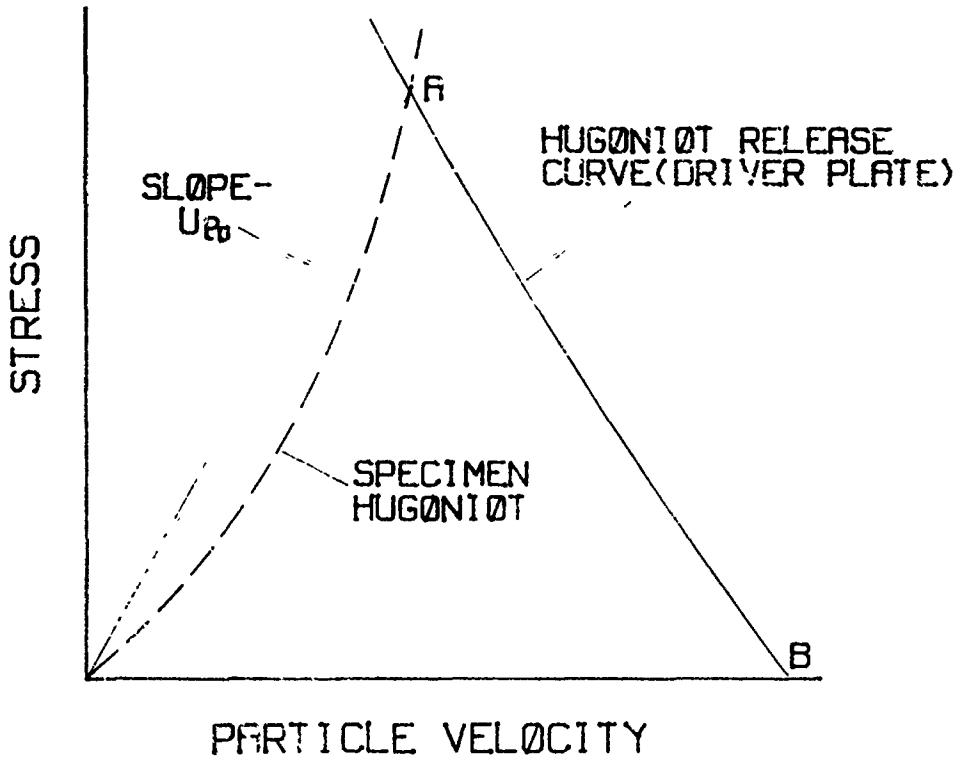

Figure 6. Schematic of impedance match method

25. Two ways are possible in attaining the state of point A. The first is used if the driver in explosives systems or impact plates in gun systems has known release curves. The free surface velocity, ufs, of the driver or impact plate and the propagation velocity, U, in the specimen are measured. The release curve of the driver is centered at B representing ufs. State A, representing the Hugoniot state in the specimen is the point of intersection between the driver release curve and the line centered at the origin whose slope is the product of U and the initial specimen density ρ_o. The specimen Hugoniot becomes the

curve which is fitted through several such points determined after several tests at other stress levels. In gun tests where the impactor plate is the same material as the specimen (symmetric impact) a measurement of impactor free surface velocity and specimen shock velocity is sufficient. In this case the particle velocity u in the specimen is exactly 1/2 u_{fs} if the impactor is stress free prior to impact. The desired state A is determined by the intersection of the line of slope U_{po} and a vertical line passing through 1/2 B.

26. If the shock is unstable, that is, has multiple-step shock fronts, TOA pins cannot be used because only the times of arrival of the leading front are registered. In this case other methods to determine individual shock front propagation velocities are necessary.

27. If these individual shock front velocities are measured, the impedance match method can be applied incrementally to determine Hugoniot states for each shock state. The impedance match method is calculated analytically by applying the conservation equations 1 and 2, the free surface-particle velocity relationship, and/or the equation of the driver or impactor release curve. This operation is readily adapted to the computer.

Electromagnetic
particle velocity method

28. The electromagnetic or induction gage[11-13] provides a direct measure of particle velocity in nonconductive material as a function of time. This gage is an "in-material" gage where the gage, either a foil or fine wire, is sandwiched within the test specimen. This technique is

shown schematically in Figure 7. The specimen material is mounted in a magnetic field so that the effective gage length is normal to the magnetic lines of force.

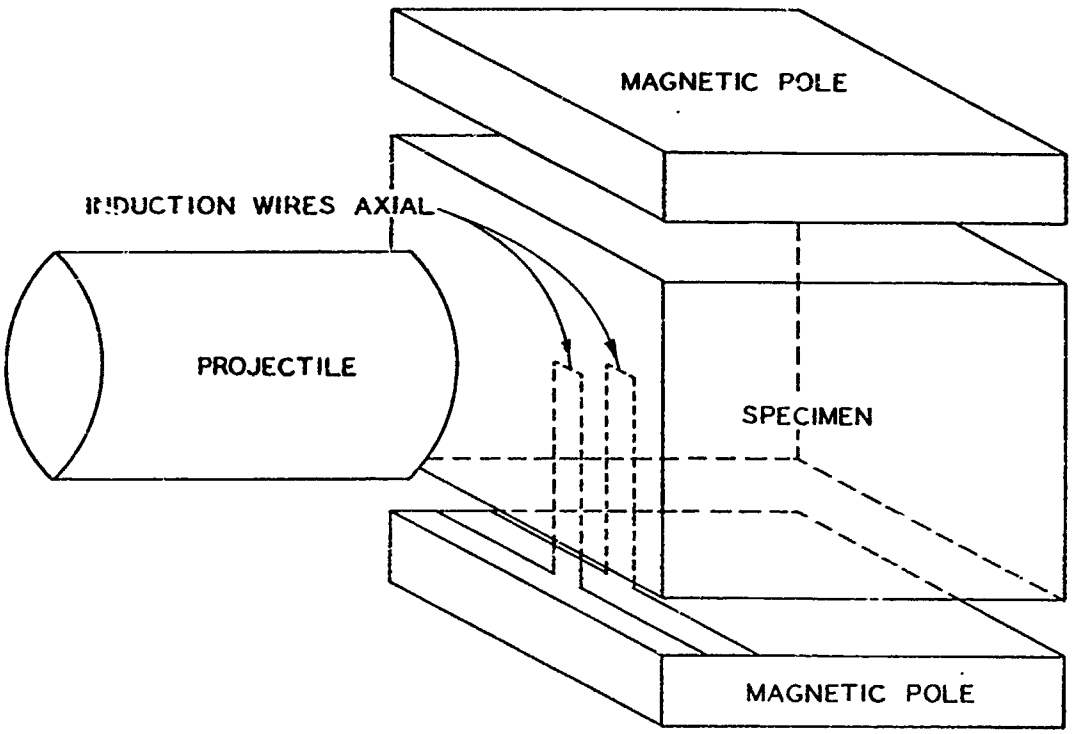

Figure 7. Schematic of induction wire particle velocity gage experimental setup

29. As a shock wave passes through the specimen the resulting material particle motion displaces each gage through a small portion of the magnetic field generating an electromotive force (emf). This emf is proportional to the particle velocity in the specimen by

$$E = Blu_p \tag{3}$$

where,

E = emf, volts

B = magnetic field strength, webers/m^2

l = effective length of wire, m

up = particle velocity, m/sec

By sandwiching several gages in the specimen along the path of shock propagation particle velocity-time records are obtained at each point. References 13 and 14 describe two incremental data reduction methods. Both are based upon the continuity equations in Lagrangian coordinates and use calculations of shock velocity at increments of particle velocities between gage records as input data.

30. An advantage of the induction gage is that the current flow in the gage is low; consequently, resistance heating that might destroy the gage during shock passage is reduced especially when inhomogeneities in the test material cause uneven displacement or shearing of the gage. The gage has very little hysteresis and therefore is ideal for measuring release states[15] (unloading). Theory dictates[16] that particle velocity gages can be used only when the shock wave is not strongly decaying with propagation distance. The requirement is that when particle velocity gages are used in a decaying shock environment the stress-time history at one[14] of the particle velocity gage positions must be monitored. The specific volume-particle velocity relationship can then be calculated. It has been found in practice, except for very strongly decaying shock behavior, that a consistent data reduction correction is possible to bring final results within experimental error when only particle velocity gages are used.

Piezoresistive "in-material" gage method

31. Certain metals or metallic[15,16] alloys when subjected to shock stress exhibit a change in resistance proportional to the stress level. These materials are piezoresistive and include manganin, ytterbium, etc. When fabricated into gages[17] piezoresistive metals can measure stress-time histories within a shocked specimen. The relationship between resistance change and stress is proportional to the piezoresistive coefficient(s) of the piezoresistive metals. This coefficient has been found to be nonlinear, proportional to the shock stress. Calibration curves have been determined to convert resistance change to stress. The curve for manganin was found to be nonlinear in the range from 0-40.9 kilobars* as shown below.

For $\sigma < 7.0$ kilobars

$\sigma = (\Delta R/R)/0.0024$ ohms/ohm/kilobar,

and for $7.0 < \sigma < 40.9$ kilobars

$$\sigma = 4.168\ (\Delta R/R) - 0.1154\ (\Delta R/R)^2 + 0.00567\ (\Delta R/R)^3 - 8.91 \times 10^5 (\Delta R/R)^4.$$

The piezoresistive coefficients for manganin[18] in the range 40.9-400.0 kilobars and ytterbium[19,20] between 0 and 15 kilobars are also known. The gages most widely used are fabricated from thin foils (typically 0.0005-in.) into a continuous line grid in various resistances and sizes. The gages are employed in a wheatstone bridge configuration with the gage acting as the active arm. A voltage is discharged across the bridge. The gage is

---

* Information obtained from L. Lee, Sandia Laboratories, Albuquerque, New Mexico.

stressed, its resistance changes causing a bridge imbalance which is recorded as a voltage-time trace. The bridge calibration[21] is applied to convert the trace to resistance change-time and finally the piezoresistive coefficient calibration is employed to convert to stress-time.

32. A commonly used manganin gage is a 50-ohm grid with a grid 0.25-in. (6.35 mm) square. Many other gage sizes and configurations have been used especially where the gage is used to measure ground shock during large high explosives and nuclear events. The smaller grid is normally used in laboratory experiments because of the limited plane wave area in laboratory EOS experiments.

33. Hugoniot states are determined from several stress gages in a manner similar to that for multiple particle velocity gages. The method is well documented in Reference 14. A major problem when using piezoresistive grids is the premature gage failure. High joule heating occurs when the gage is activated. Grid imperfections and unequal particle motion displacements of portions of the gage in inhomogeneous materials cause localized hot spots which can easily "burn out" the gage. This problem has been somewhat solved by encapsulating the gage within thin layers of epoxy-fiberglass, ceramic materials, or metals. Encapsulating is also employed to reduce stretching of the gage due to lateral material flow. Encapsulating increases the accuracy of the gage by reducing the strain gage effect. The major advantage of piezoresistive gages is that they can be used to directly measure stress-time profiles along the path of shock propagation.

Stress reflection method

34. The stress-reflection method is a technique using piezoresistive stress gages where the Hugoniot state is determined by the impedance mismatch between the subject material and a witness material. The method has been used successfully to determine partial EOS for soils,[22,23] volcanic tuff,[24] and EOS rock-matching cement grouts.[25] The stress reflection method was developed to test friable materials or those materials with relatively large grain sizes. A schematic drawing illustrating this method is shown in Figure 8A. A manganin foil is sandwiched between two disks of a homogeneous witness material with a known EOS that has a slightly lower slope than that estimated for the specimen material. Plexiglas has been used as the witness material. The specimen material is placed in intimate contact with the Plexiglas assembly.

35. The input stress in the witness material and the equilibrium stress in the specimen material appear as two steps in the witness gage stress-time record as illustrated in Figure 8B. The second step is a result of a shock wave traveling back toward the impact surface due to an impedance mismatch at the witness-specimen interface. Data analysis is accomplished by the impedance match technique. An advantage of this method is that large, localized differential particle velocities are eliminated for large grained materials. Measurement of the stress wave after propagation through the specimen is eliminated. Consequently, the need for a long input shock pulse is reduced. Accuracy can be

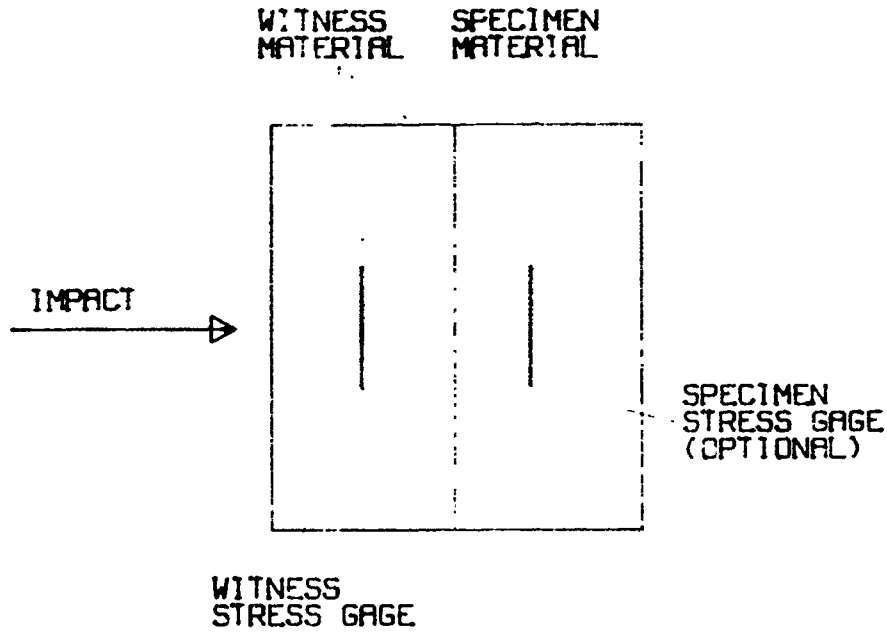

Figure 8A. Schematic of stress reflection method test specimen

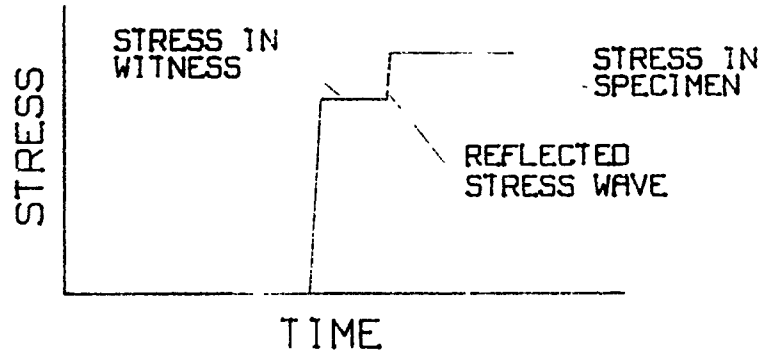

Figure 8B. Typical stress-time record from witness stress gage in stress reflection method

enhanced in several ways. If the gage area is small relative to the specimen grain size, several gages can be placed within the witness material and the results of the gages averaged. Accuracy can also be enhanced by using larger area gages. One disadvantage of the stress reflection method is the difficulty in obtaining intermediate specimen Hugoniot states at stress levels where multiple wave shocks exist.

Other measurement methods

36. Several other measurement methods have been used to obtain EOS data. These include the plane and inclined mirror streak camera,[26,27] laser velocity inferometer,[28] and X-cut quartz gage[29] techniques. All of these are proven techniques and are widely used. However, in-material gage methods are becoming most popular because of their versatility.

PART IV: CONCRETE MIXTURES

37. The concrete mixtures used in this work were developed at the U. S. Army Engineer Waterways Experiment Station (WES) for a prior study,[30] but were well suited to accomplish the present objectives. These mixtures included a prototype 3/4-in. maximum size aggregate concrete and a 1/8-in. maximum size aggregate concrete specifically designed to match the EOS and other physical and material properties of the prototype mixture.

38. Physical properties documentation including EOS determinations were available for the 1/8-in. mixture (mixture 6A). A lesser amount of data were available for the 3/4-in. mixture (mixture 75A) excluding EOS determinations.

39. Type II portland cement (RC-602) was used in these mixtures. Both mixtures contained crushed granite coarse aggregate from the Cheyenne, Wyoming, area. Natural sand also from the Cheyenne area was used as the fine aggregate. Mixture proportions and other mixture data for mixtures 6A and 75A are shown in Tables 1 and 2 as follows:

Table 1. Concrete Mixture Proportions

Material	Solid Volume, cu ft		Saturated Surface Dry Weight, lb	
	6A	75A	6A	75A
Portland cement	4.072	4.072	799.00	799.00
Coarse aggregate	9.212	10.200	1503.67	1664.95
Fine aggregate	6.670	7.386	1092.88	1205.62
Water reducing admixture Pozzolan No. 8	--	--	2.125	--
Water	7.046	5.342	438.99	332.78
	27.000	27.000	3836.66	4002.35

Table 2. Concrete Mixture Data

	Mixture No.	
	6A	75A
Maximum aggregate size, in.	1/8	3/4
Sand-aggregate, percent vol.	42	42
Bags cement/cubic yard	8.5	8.5
Water-cement ratio by wt.	0.55	0.42
Slump, in.	3-1/2	2-1/2

The proportion relationships shown in Table 2 differed basically only in water content.

40. The water content of mixture 6A was increased over that in mixture 75A for reasons of workability. Considerable effort was spent to reduce the amount of entrapped voids (1/8 - 3/16 in. typical size) in the small aggregate mixture. Through a combination of proper water/cement ratio, addition of a water-reducing admixture, and internal vibration for 10 minutes an acceptable product was attained without segregation of aggregate particles. Test specimens for the determination of physical properties for mixture 6A and the EOS samples for mixture 75A were obtained by coring the applicable 32- by 24- by 15-in. cast blocks. It was determined that cores from a large block would provide more consistent results when compared with cast cylinders.

41. These mixtures were designed to match each other in material properties, especially compressive strength. However, since mixture 6A was to be subjected to high levels of radiation in the prior study, the mixtures were also designed to match each other in elemental composition. Physical and chemical properties and elemental composition are shown in Tables 3, 4, and 5, respectively.

42. The chemical analyses for the mixtures are based upon analyzing the constituent materials individually, then are recalculated based on mixture proportions.

Table 3. Concrete Physical Properties

Physical Properties	Mixture Number 6A	75A
Compressive Strength, psi		
7 days	3847	5130*
28 days	6100	6800*
90 days	7580	8180*
Poisson's Ratio	0.165	
Static E, psi x 10^6	3.31*	
Dynamic E, psi x 10^6	4.32	
Compressive Wave Velocity, ft/sec	12,945	
Thermal Diffusivity, cm^2/sec	0.0077	
Specific Heat, cal/gm - C^o	0.23	
Thermal Conductivity, cal/sec - cm - C^o	0.0041	

* 6- by 12-in. cylinders. Remainder cores from 32- by 24- by 15-in. cast blocks.

Table 4. Chemical Analysis of Concrete Materials

Oxide	Percent Oxide Present		
	Cement (RC-602)	Wyoming Granite	Wyoming Natural Sand
SiO_2	21.79	72.18	76.27
Al_2O_3*	5.11	14.08	13.05
Fe_2O_3	4.55	2.75	1.28
MnO	0.08	0.01	0.01
TiO_2	0.23	0.20	0.11
P_2O_5	0.46	0.05	0.08
CaO	63.18	1.90	1.50
MgO	0.83	0.02	0.14
Na_2O	0.11	2.48	2.44
K_2O	0.44	3.92	2.64
SO_3	2.05	--	--
Insoluble Residue	0.13	--	--
Moisture	0.55	0.17	0.16
Ignition Loss	1.34	0.52	0.68
	100.17	98.23	98.36

* Results calculated on dried (105°C) sample basis. Ignition @ 850°C.
$Al_2O_3 = K_2O_3 - Fe_2O_3 - TiO - P_2O_5$

Table 5. Elemental Composition of Mixtures 6A and 75A

Element	Percentage Composition (Wt) Mixture 6A	Mixture 75A
Oxygen	50.43	49.13
Silicon	25.51	26.63
Calcium	10.25	10.21
Aluminum	5.45	5.71
Potassium	1.98	2.10
Iron	1.67	1.74
Hydrogen	1.31	0.95
Sodium	1.25	1.32
Sulfur	0.17	0.17
Magnesium	0.13	0.13
Titanium	0.09	0.10
Phosphorus	0.06	0.06
Manganese	0.02	0.02
	98.32	98.27

PART V: COMPUTER STUDIES

43. Numerical wave propagation simulations were performed using TOODY I, a two-dimensional wave propagation computer code. Use of this code was aided by earlier work by B. R. Sullivan.[31] The code available for use was an earlier version[32] developed by Sandia Laboratories. It was designed for use on the C.D.C. 3600 with two 32K core banks or the C.D.C. 6400/6600 computers with storage capacities of 68,000 decimal (204,163 octal) locations. The code was converted to the Honeywell 635 system at WES during the course of the present work. Computer hardware limitations precluded use of later versions of TOODY. However, it was determined that the capabilities of TOODY I were sufficient to carry out the program objectives.

44. The basic objective of the computer simulations was to study the waveforms and wave interactions in a computer model of concrete. This information was needed to aid in experimental design especially in regard to gage placement including gage spacing relationships.

45. The computer models consisted of a grid in the r-z plane with unit thickness in the r-θ plane. The rectangular grid was divided into meshes where i represents the location of meshes in the z direction (direction of shock propagation) and j the location in the r direction. Figure 9 depicts a typical mesh grid. The specimen material occupies the interior meshes. The pressure input, symmetric centerline and free surface boundary conditions are specified by the boundary meshes. The code can be used with up to 10 different components in a model. Figure 9 simulates flat plate impact at the pressure input boundary.

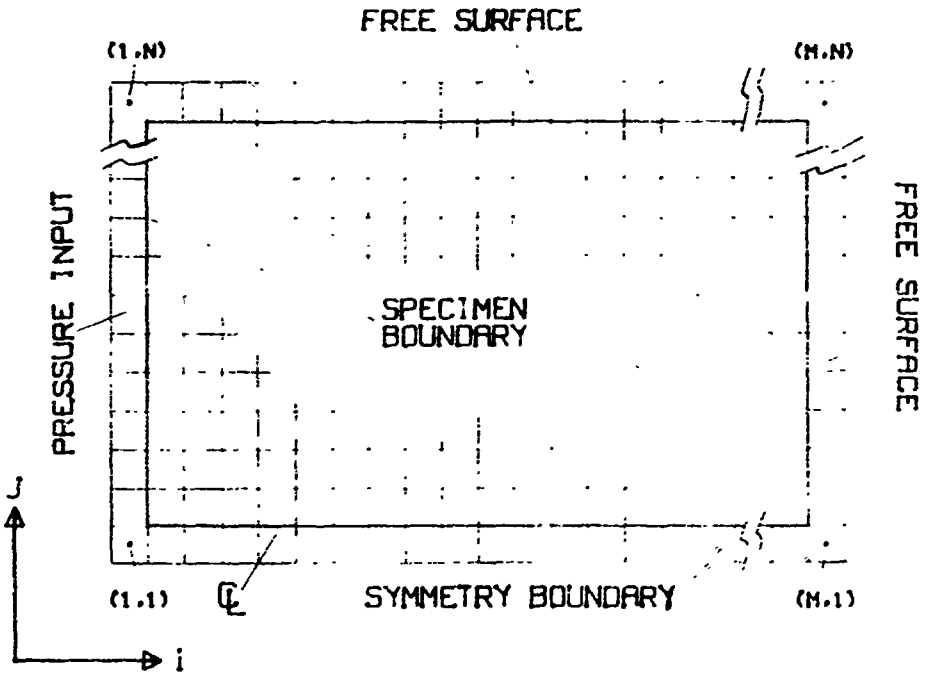

Figure 9. Diagram of TOODY mesh grid

46. The pressure input to the code is a flat-topped step (0 microsecond rise time). The program spreads the step over the first several meshes. In this study the typical rise time to 90 percent of the peak stress was 0.2 microseconds in the first material mesh ($i = 2$). Preliminary computer runs showed that smaller mesh sizes reduced the initial rise time and produced a more stable waveform. Rise time and waveform stability are also functions of a mathematical artificial viscosity term in the calculation. The artificial viscosity term describes waveform relaxation in the model. The details of the calculation method are not discussed here since they are well documented in References 31 and 32.

47. The computer study resulted in five production runs including one each modeling mixture 6A, the concrete matrix for mixture 75A, and the granite aggregate. The remaining two runs were conducted on models of the 75A mixture with different spacial arrangement of the aggregates. For the purposes of this study and in particular in the computer modeling work, the term concrete matrix is defined as the entire concrete system excluding all aggregate sizes greater than 1/8 in. Over 20 additional computer runs were conducted to check out mesh size relationships, determine the correct material property input values and their effects on calculation stability and accuracy. All production runs were conducted with an input pressure step of 10 kilobars. An initial equilibrium stress of $\approx$ 7.5 kilobars was observed. Several of the experimental tests (to be described later) were conducted at the same stress levels for comparison.

48. Computer simulation runs 1 and 3 for mixture 6A and the Wyoming granite, respectively, were subject to verification with actual data. The actual response of the concrete matrix modeled in run 2 was unknown; consequently, the calculated waveforms desired were estimated using the response of mixture 6A as a basis for comparison. The estimated material properties of the concrete matrix of mixture 75A were determined by a procedure that involved a simulated removal of the coarse aggregate and estimating the properties of the resulting mixture, assuming an air dry final product. The resulting concrete matrix had $\approx$ 50 percent less aggregate per unit volume than did mixture 6A. With the coarse aggregate

removed the proportion of cement and water per unit volume was almost doubled in the matrix. However, when considering the air-dry state in which much of the water was removed it was concluded that more water per unit volume would be released from the matrix material than from 6A. It was then also concluded that the compressive strength, hence, the HEL of the matrix would be higher than that of 6A. This assumption has been somewhat verified by triaxial tests[33] in which the resistance to shear was found to be greater for dry specimens. The HEL of the matrix was then estimated to be $\approx$ 1.75 kilobars compared with $\approx$ 1.25 kilobars for mixture 6A. Each of the production runs 1-3 was the last of a series of runs to model the subject material. Some difficulty was encountered in properly modeling the granite. The calculation tended to become unstable outside a very narrow band of input parameter values. The mesh grid model for runs 1, 2, and 3 consisted of 73 meshes in the z direction (i = 2-74) and 23 meshes in the r direction (j = 2-24). The boundary meshes were as described earlier and depicted in Figure 9. Mesh dimensions that produced the most stable calculation and used in all production runs were z = 0.25 mm and r = 1.0 mm. The materials in runs 1-3 were considered homogeneous and no attempt was made to model the aggregate in the concretes for runs 1 and 2. Figures 10-12 are stress-time profiles for runs 1-3, respectively. These waveforms were taken along a line j = 2 where i = 2, 14, 36, 38, 50, and 62.

49. Computer runs 4 and 5 were conducted on two composite models of mixture 75A. The difference between the models was the position of the

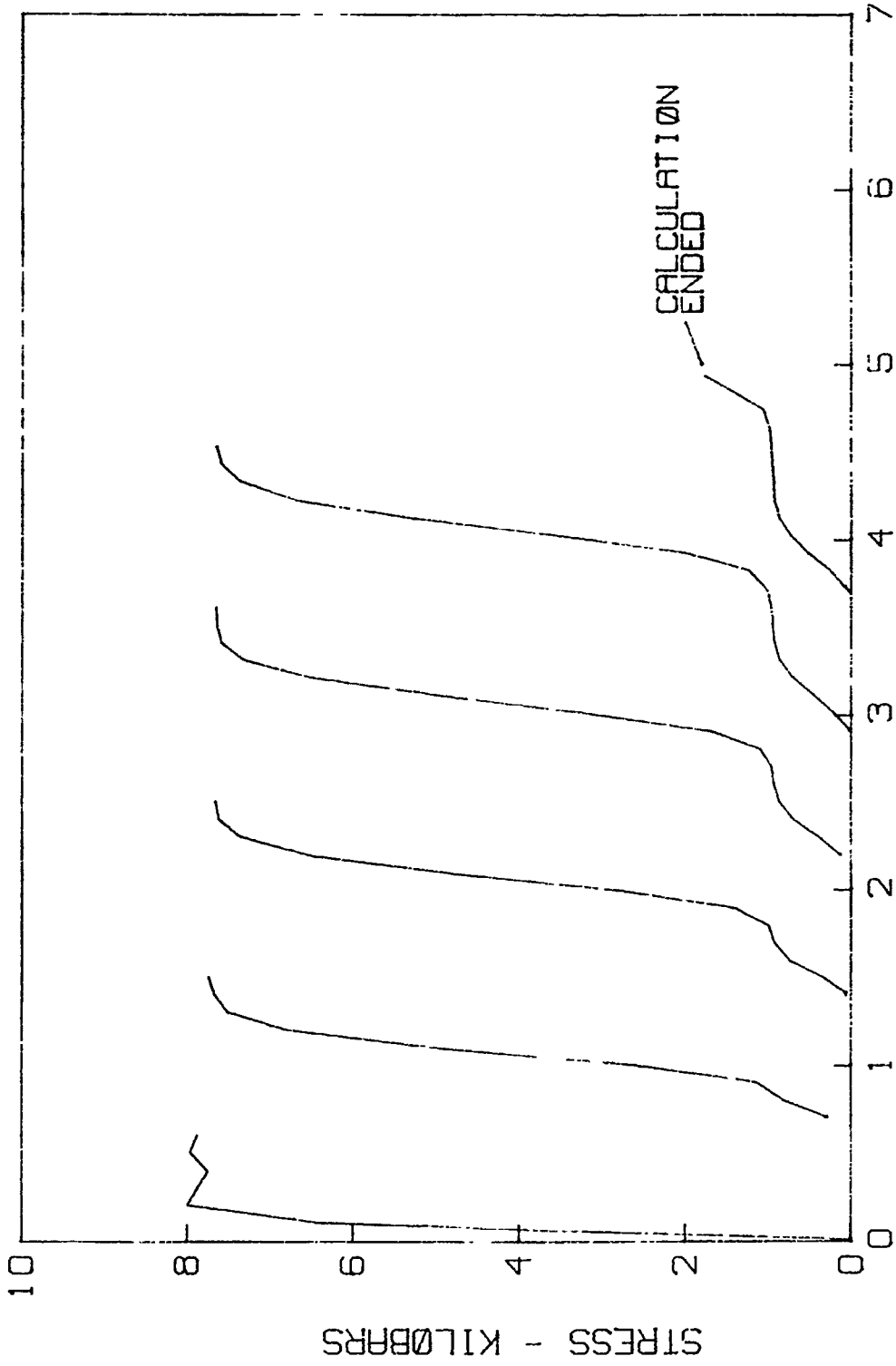

Figure 10. Computer simulated stress-time profiles for 6A concrete

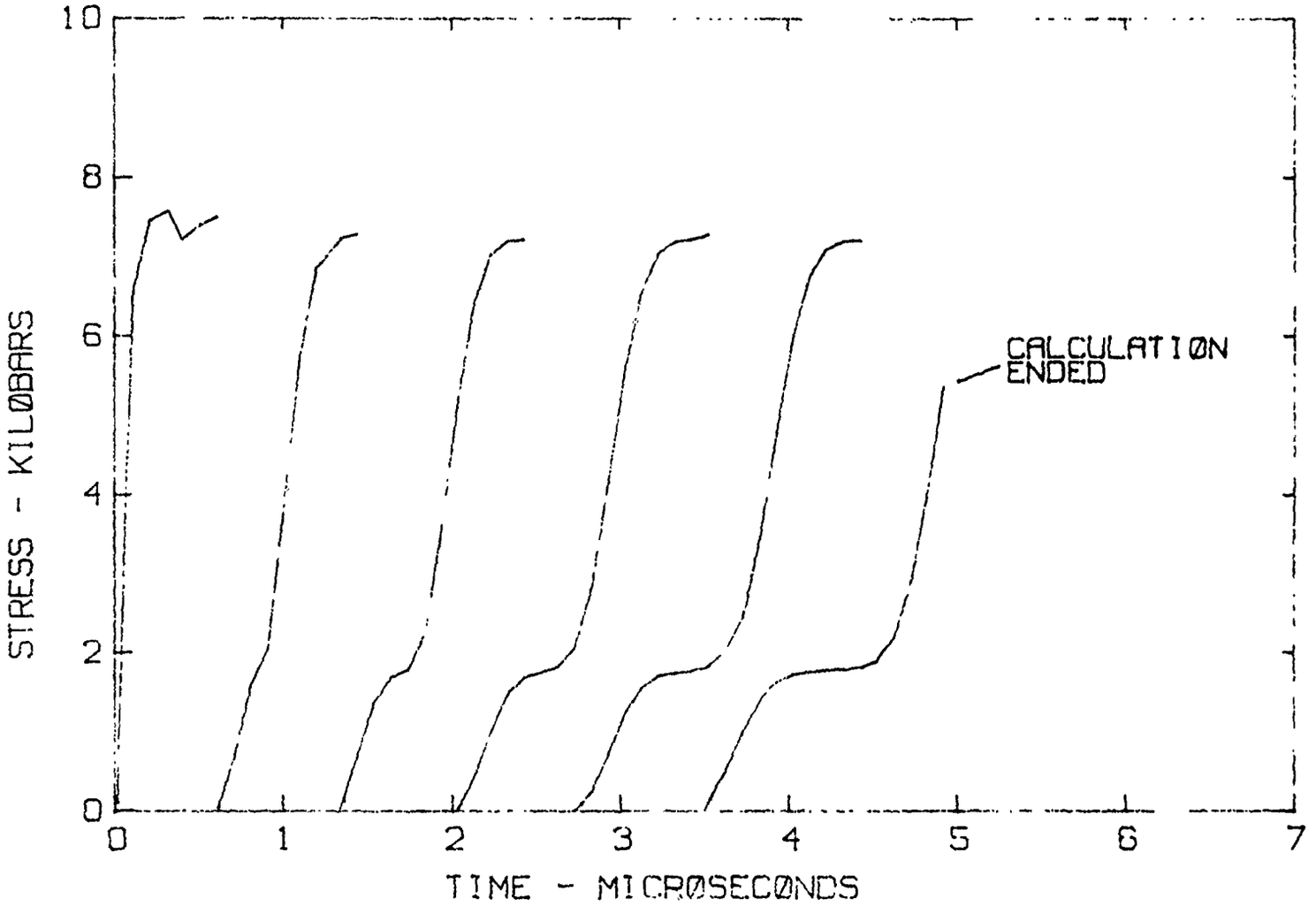

Figure 11. Computer simulated stress-time profiles for 75A concrete matrix material

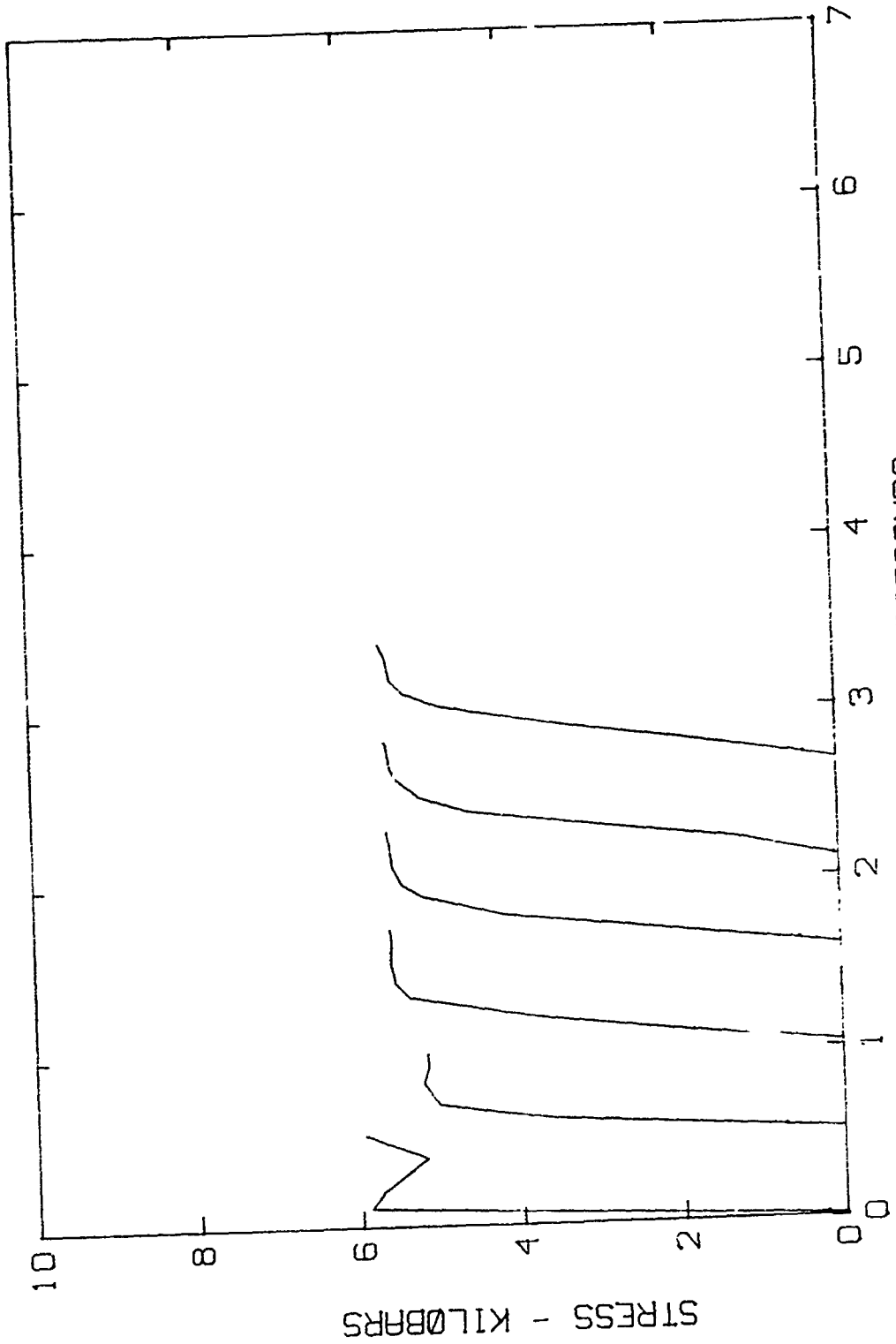

Figure 12. Computer simulated stress-time profiles for Wyoming granite

coarse aggregate within the model. The mesh grid model for these runs consisted of 88 meshes in the z direction (i = 2-89) and 23 meshes in the r direction (j = 2-24). This model was extended in the z direction compared to those used in runs 1-3 to delay effects caused by reflection of the wave from the back free surface boundary at i = 90, j = 1-25. Figures 13 and 14 illustrate the layout of the aggregate in the concrete matrix for runs 4 and 5, respectively. The cross-section area of aggregate used in the model was the average cross-sectional area of aggregate greater than 1/8 in. actually determined from cut sections of mixture 75A. The average area of aggregate was 43 percent of the total area. Mixture 6A was used in meshes i = 2-9 as the media for transporting the stress wave from the pressure boundary to the composite section of the model. This was done to be assured that the stress wave would be stable as it entered the composite concrete model.

50. A portion of the results of computer runs 4 and 5 are shown in Figures 15-18. Figures 15-17 depict the variation in wave profiles for wave propagation along differing material paths in the direction of propagation. Each of the figures shows a series of stress-time profiles along lines j = 2 and j = 6 (lines AB and CD, Figure 13) of run 4 and line j = 2 (line AB, Figure 14) of run 5 at i = 2, 9, 16, 23, 30, 37, 44, 51, 58, 65, and 72.

51. Figure 18 from runs 4 and 5 shows stress-time profiles produced by averaging the stress-time profiles of meshes j = 2-15 along lines i = 16, 30, 44, and 58 normal to the direction of wave propagation. The positions

of these lines in the model are shown in Figures 13 and 14 by lines I, II, III, and IV, respectively. These wave profiles represent the output of a 1.4-cm stress gage at these positions.

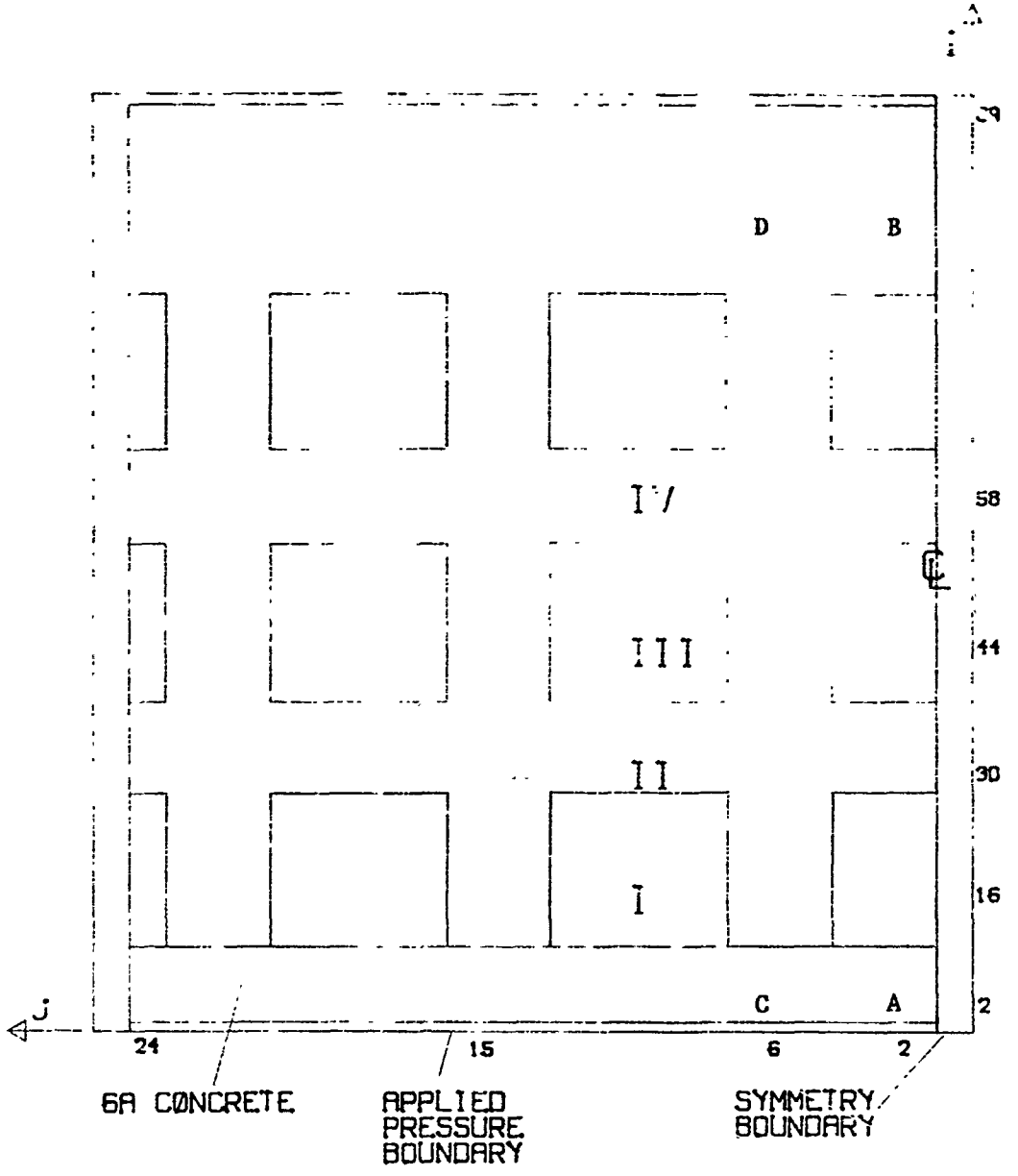

Figure 13. 75A concrete composite computer model 1

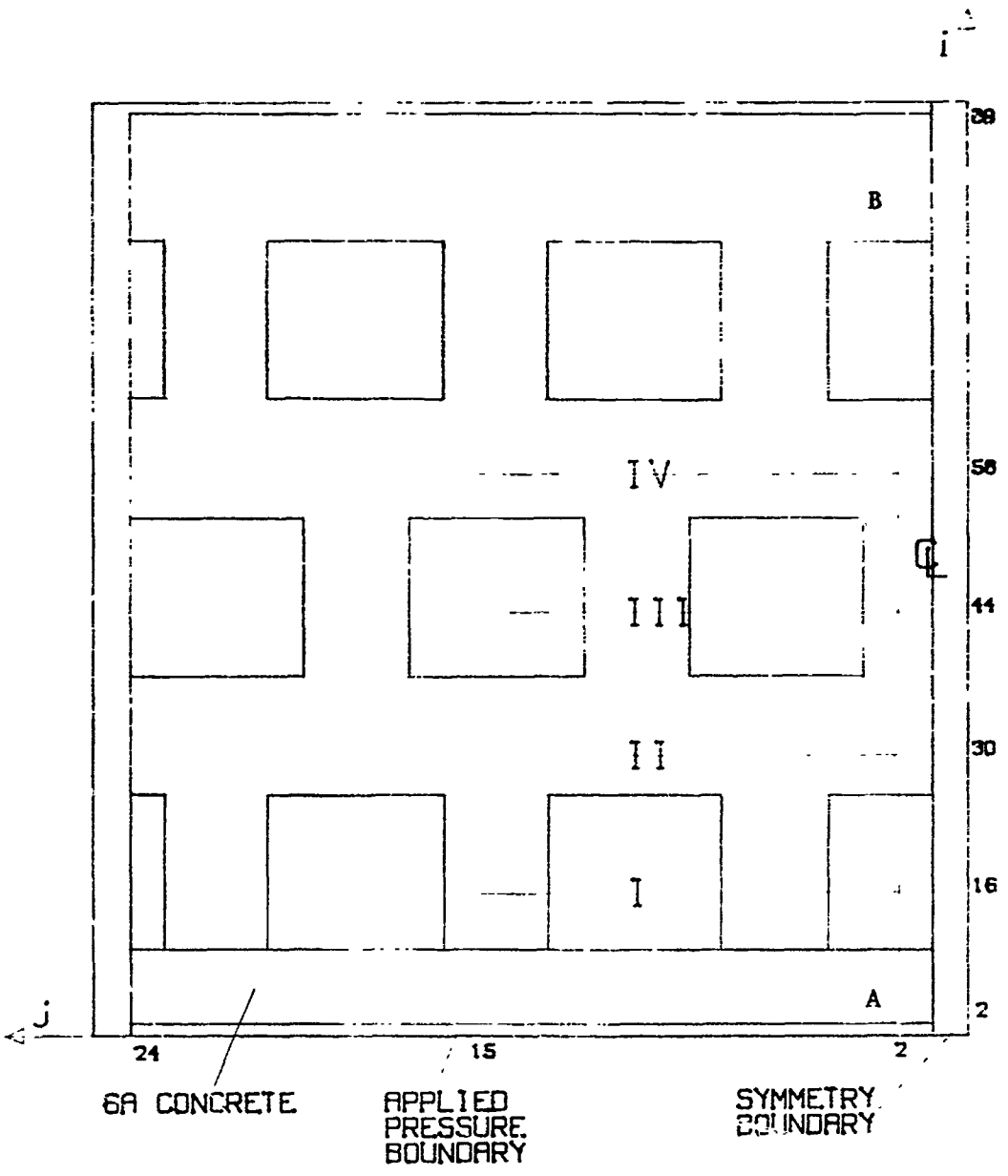

Figure 14. 75A concrete composite computer model 2

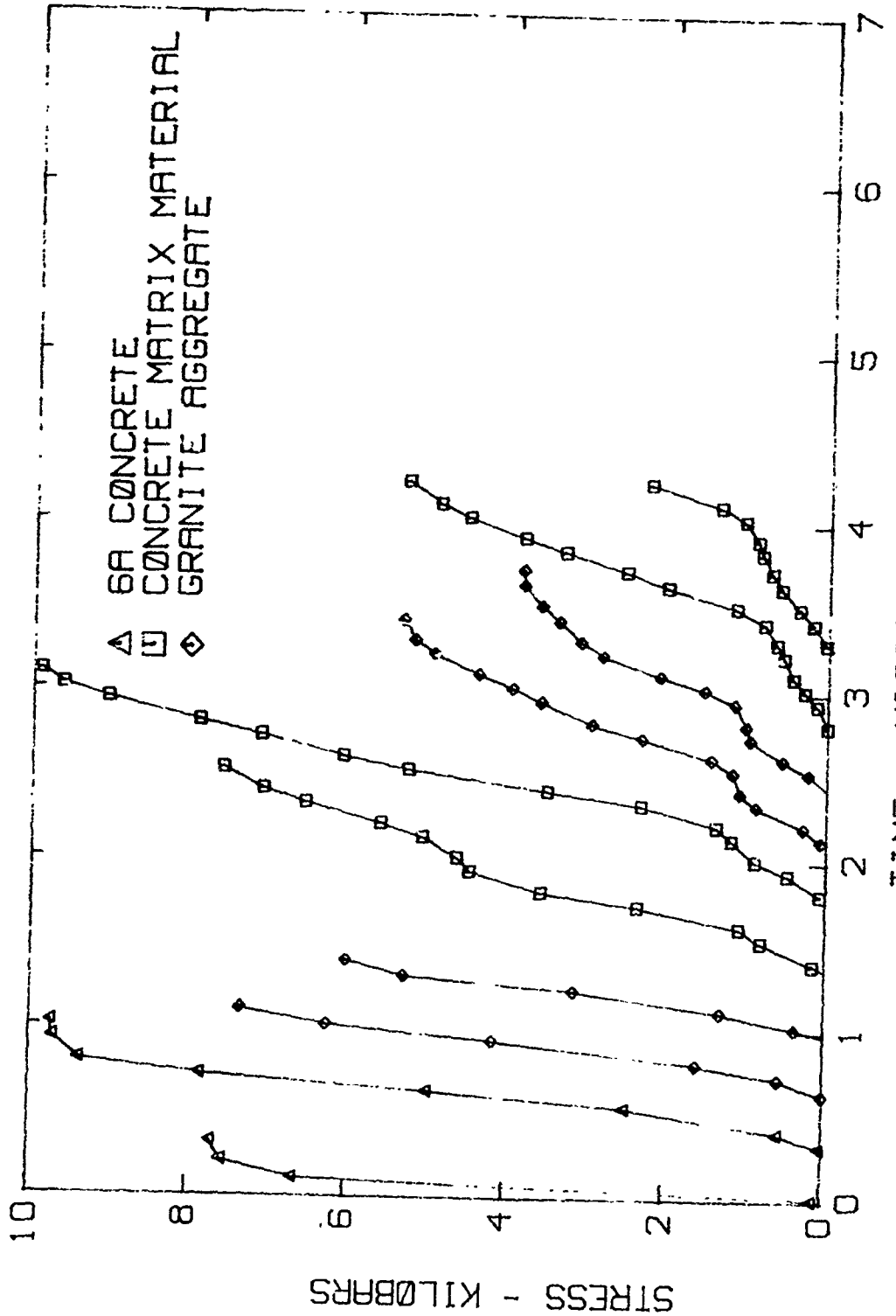

Figure 15. Computer simulated stress-time profiles along line J = 2 in 75A concrete composite model 1

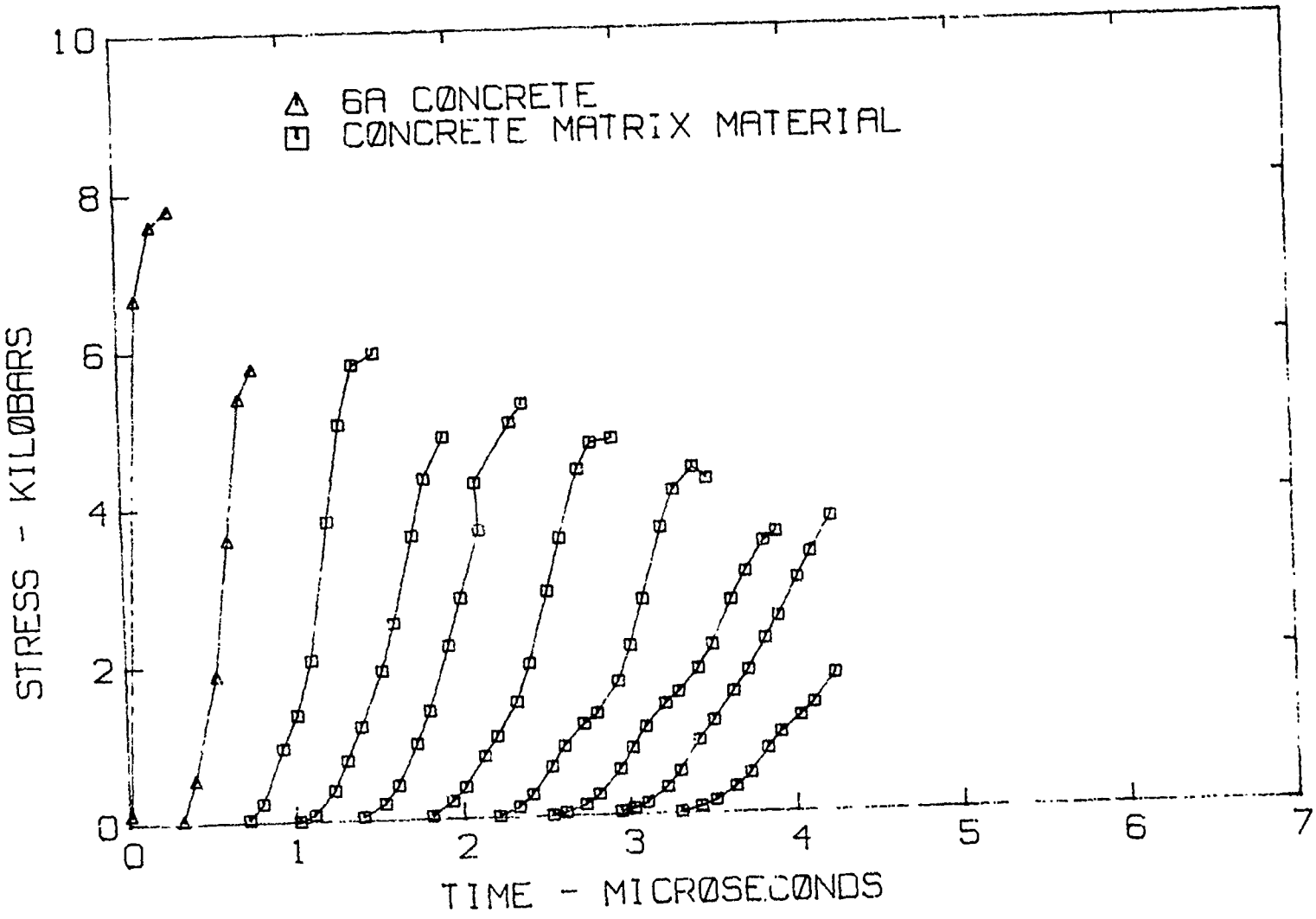

Figure 16. Computer simulated stress-time profiles along line J = 6 in 75A concrete composite model 1

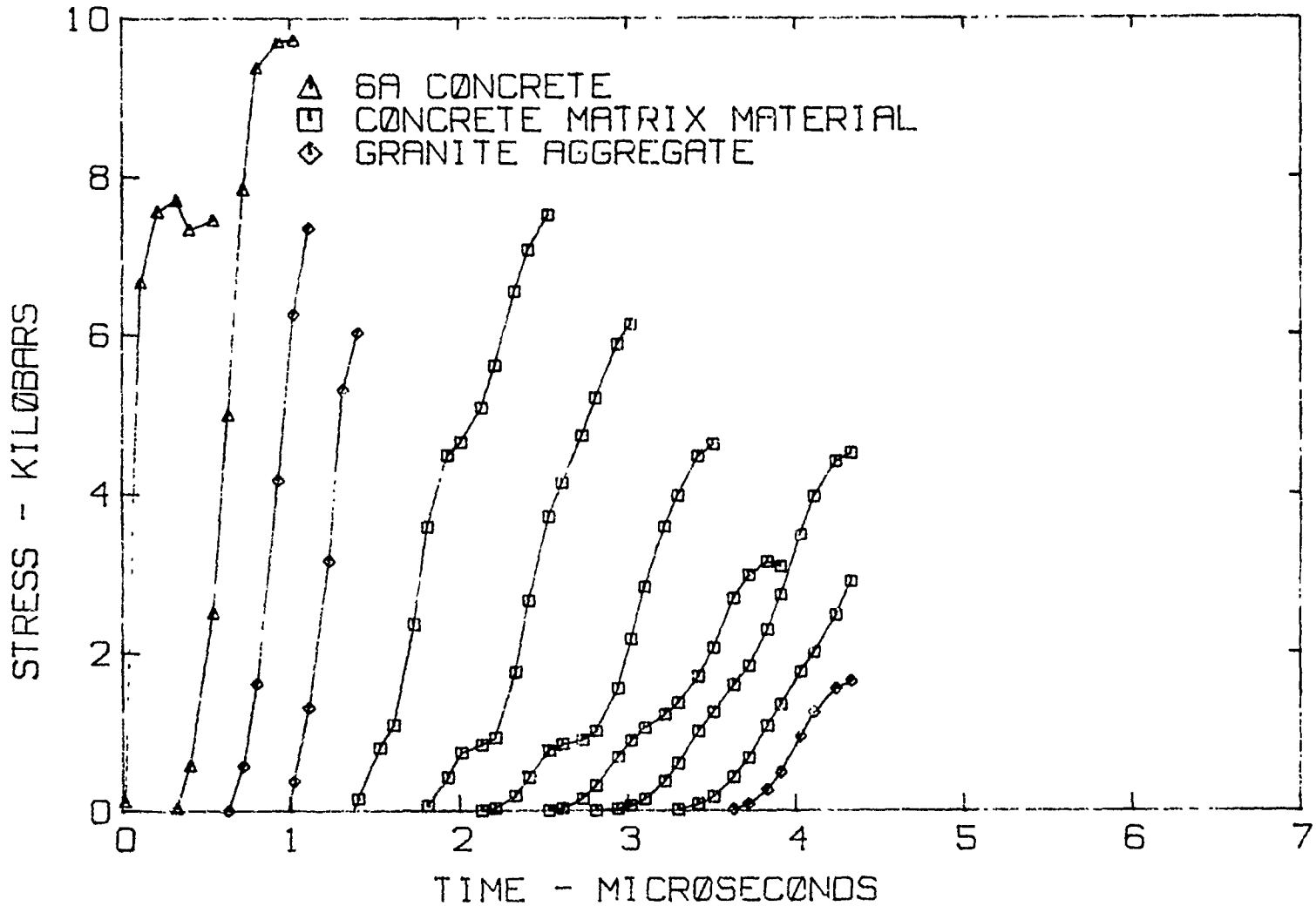

Figure 17. Computer simulated stress-time profiles along line J = 2 in 75A concrete composite model 2

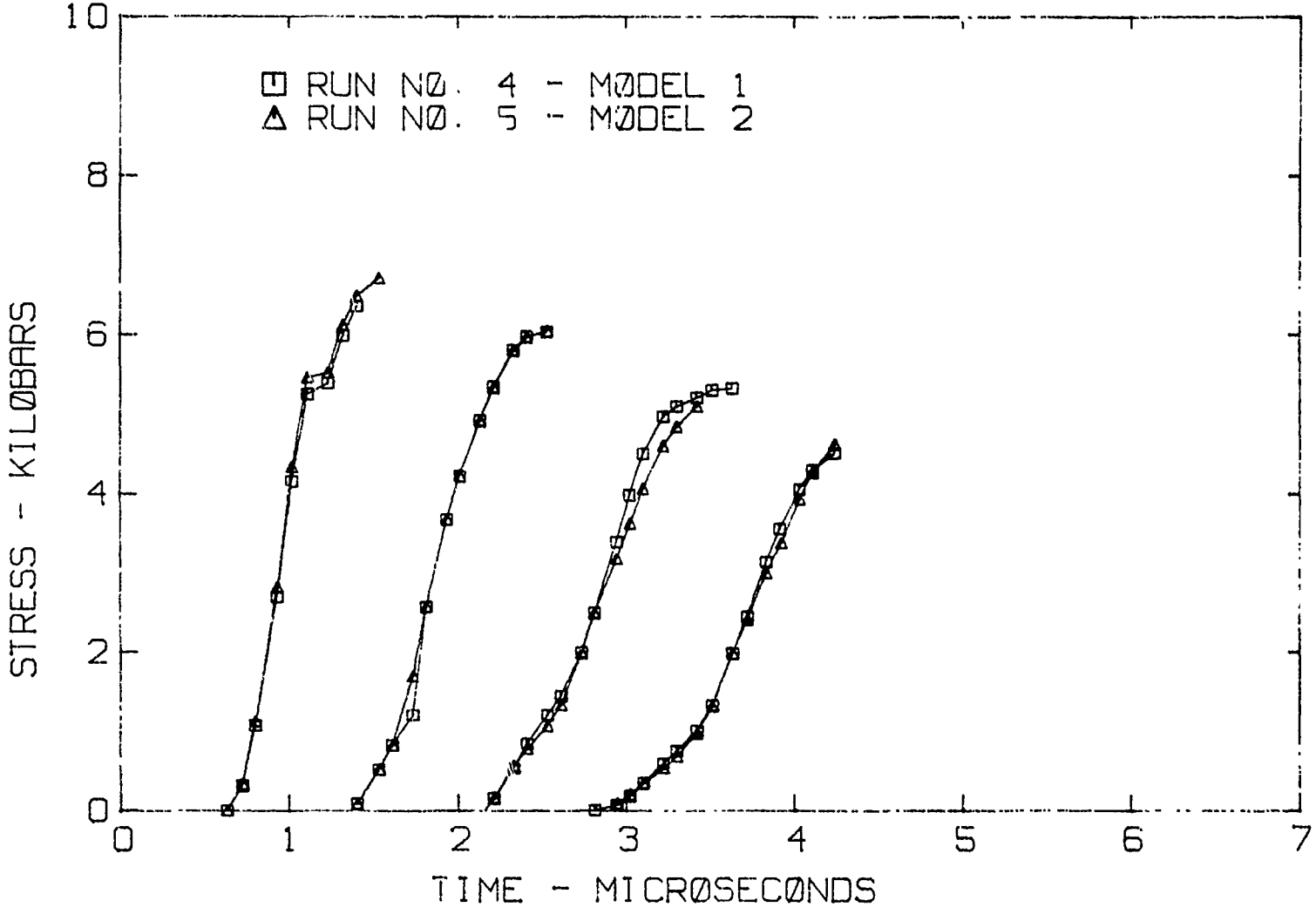

Figure 18. Computer simulated stress-time profiles averaged from positions along lines I, II, III, and IV in 75A concrete composite models 1 and 2

PART VI: EXPERIMENTAL STUDIES

52. This section describes the equation-of-state tests conducted during the course of this study. Test shots 1045 and 1050 were conducted on mixture 6A to supplement previously documented data.[30] Test shots 1091-1096 were conducted on mixture 75A to establish the initial EOS documentation for that mixture in the range of 0-10 kilobars. Results of these shots are tabulated in Table 6. Stress-particle velocity and stress-volume states attained are shown in Figures 19 and 20, respectively. It was recognized that this stress range is somewhat limited; however, it was felt that more tests were desirable within a limited stress range to more precisely define the problem areas and low stress EOS. In addition, it was expected, due to the probable existence of multiple-wave shock response, that this stress range would be the most difficult in which to obtain accurate data.

53. All tests were conducted using the Concrete Laboratory gas gun facility, which gun has a 51-mm bore diameter. It was recognized from the outset that this bore diameter was smaller than desired, but would be sufficient with careful specimen design. The projectiles were machined from high density (1.35 g/cc) polyethylene. Impact disks of 2024-T4 aluminum were machined to 1-in. thicknesses and bonded to the polyethylene projectiles. Coaxial shorting (time of arrival) pins were used to trigger the electronics a few microseconds prior to impact.

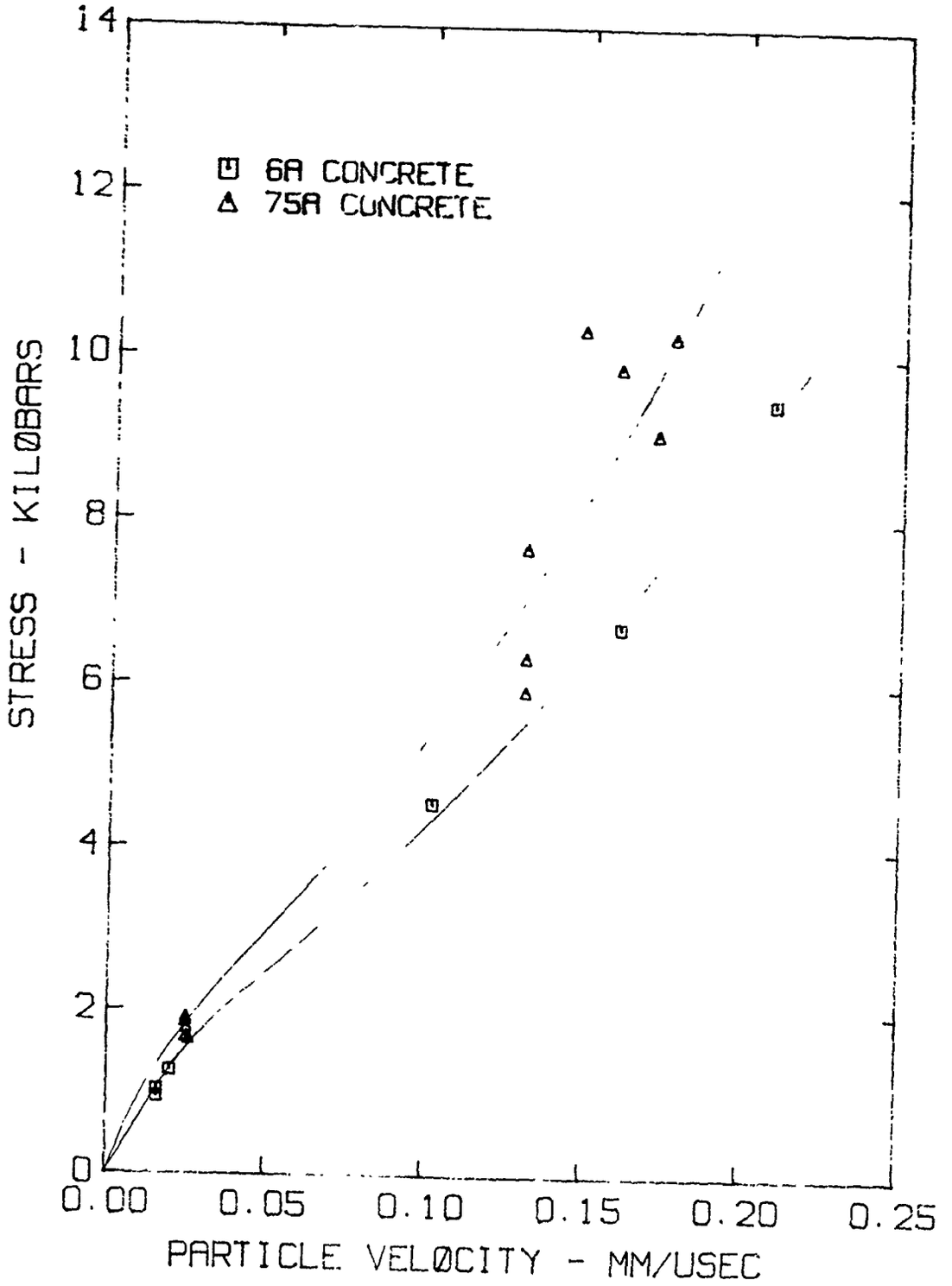

Figure 19. Experimental stress-particle velocity Hugoniot states for 6A and 75A concrete

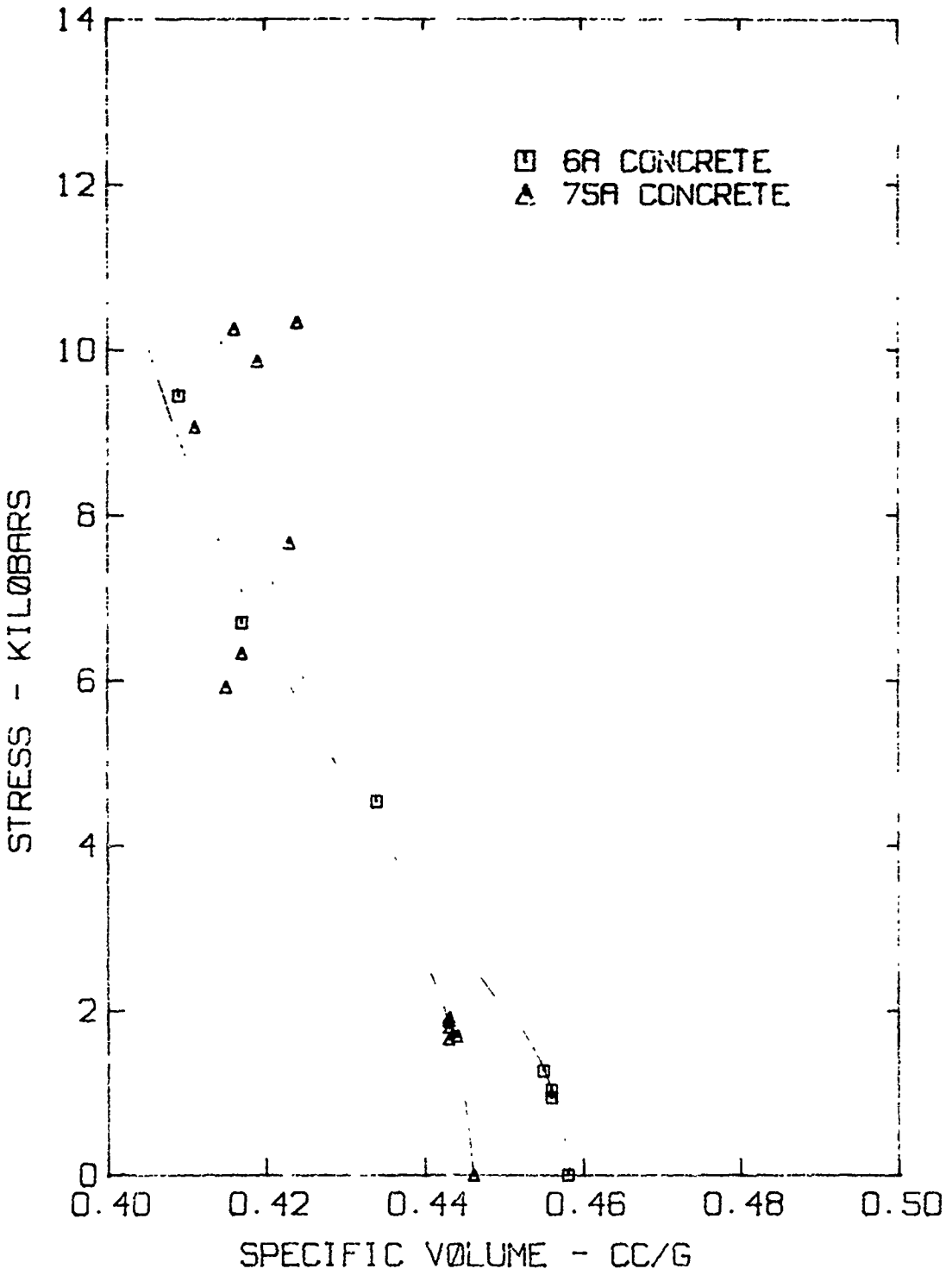

Figure 20. Experimental stress-specific volume Hugoniot states for 6A and 75A concrete

Table 6. Hugoniot Test Results

Shot No.	Concrete Mixture No.	Gage Type	HEL State				Final State			
			U_p †	u_p	σ_p	V_p	U_F ††	u_F	σ_F	V_F
1048	6A	Part. Vel.	3.47	0.020	1.26	0.455	1.82	0.209	9.44	0.409
1048A	6A	Stress	4.01	0.016	1.03	0.456	1.64	0.161	6.70	0.417
1050	6A	Part. Vel.	3.92	0.016	0.94	0.456	1.72	0.102	4.53	0.434
1091	75A	Stress*						0.177	10.25	0.416
1092	75A	Stress	4.01	0.025	1.79	0.443	2.02	0.172	9.06	0.411
1093	75A	Part. Vel.	4.18	0.025	1.88	0.443	2.22	0.131	7.66	0.423
1094**	75A	Part. Vel.	3.82	0.026	1.65	0.443	1.62	0.131	5.92	0.415
	75A	Part. Vel.	3.53	0.025	1.68	0.444	1.77	0.131	6.33	0.417
1095	75A	Part. Vel.	4.14	0.025	1.91	0.443	2.45	0.160	9.86	0.419
1096	75A	Part. Vel.	3.78	0.025	1.87	0.443	2.87	0.178	10.33	0.424

* Stress reflection method.
** Two sets of gages, one pair each at three specimen depths--one gage failed.
† Propagation velocity--leading edge of front.
†† Average propagation velocity of second wave.

54. Three in-material manganin foil stress gages mounted $\approx$ 5, 10, and 15 mm from the impact surface of the specimen were used to measure stress-time profiles in test 1048A on mixture 6A and in test 1092 on mixture 75A. In each shot one stress gage failed prematurely. Data analysis was accomplished using the Lagrangian technique noted earlier in Reference 14.

55. The stress gages were photo-etched from 0.0005-in. manganin foil then bonded between two 0.002-in. protective layers of epoxy-fiberglass. The foil grid was 0.25-in. square. The encapsulated gage was found to possess superior survival during shock transit over unprotected gages. It was found that maximum gage survival occurred when the gage leads were brought out to the back of the specimens through holes[34] drilled for that purpose (technique 1). The alternative method (technique 2) was to attach leads to the extension of the foil at the edge of the specimen. A schematic drawing of the two techniques is shown in Figure 21.

56. The reason for increased survival with technique 1 is that the foil leads did not cross the limits of plane wave area illustrated by the plane wave cone in Figure 21. Outside the cone a sharp transition in particle motion occurs due to unloading from specimen boundaries. This transition causes the foil leads in technique 1 to be subjected to localized shear and stretching. Because of the high current flow in the foil, the lead deformation causes localized areas of high resistance, hence, high heat that severs the leads. When technique 1 is used, the lead holes are positioned so that the plane wave cone will not cross the foil leads at the time the shock wave reaches the plane of the gage.

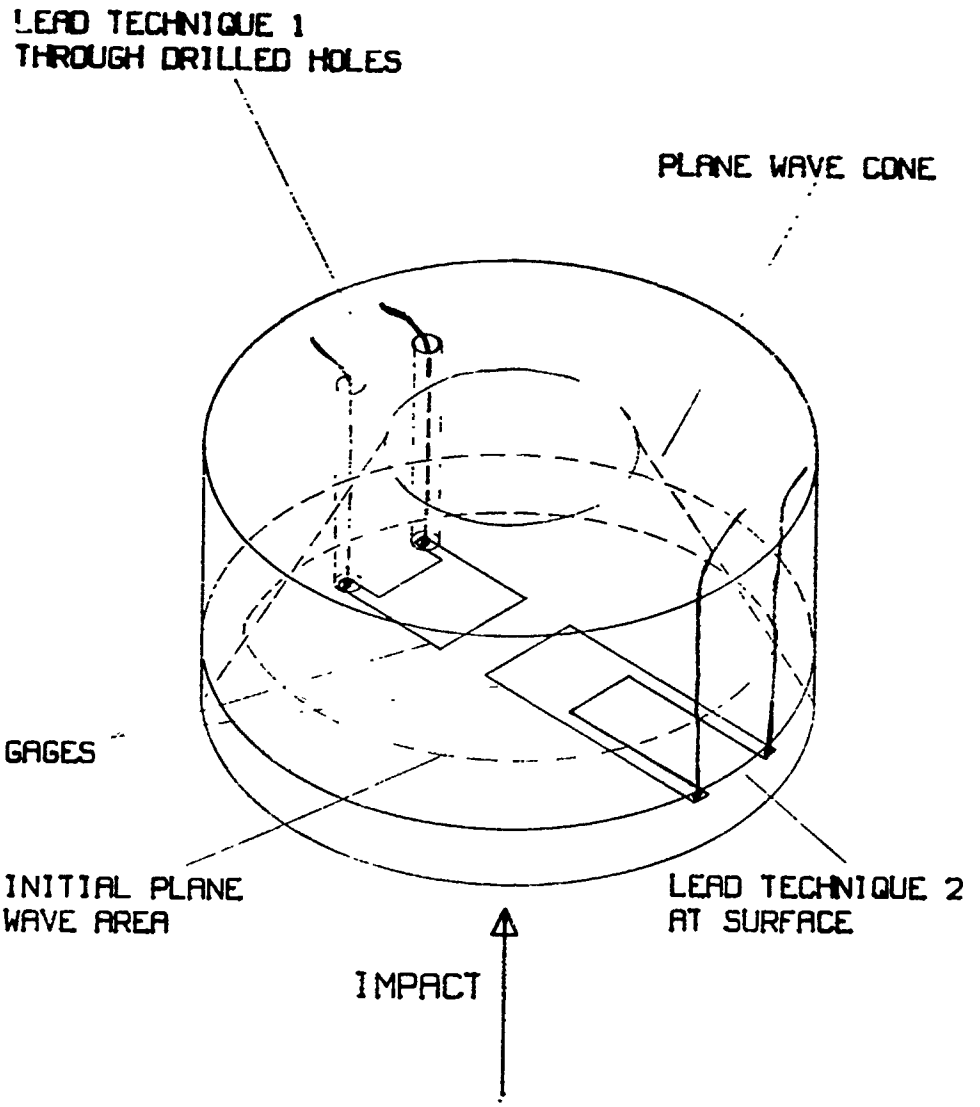

Figure 21. Illustration of techniques to bring gage leads from specimen

57. Metrophysics model 50-75C bridge power supplies were used to apply voltages across the manganin gage circuits. The outputs from the gages were recorded on Tektronix 556, 555, and 551 oscilloscopes. The trigger signal from the test specimen was first used to trigger the power supplies. Then after a delay of several microseconds the oscilloscopes were triggered. Impact ensued within a few microseconds. The reason for delay in triggering the oscilloscopes was to produce a level baseline at the beginning of the oscilloscope traces.

58. Particle velocity induction wire gages were used to measure particle velocity-time profiles in shots 1048, 1050, and 1094-1096. Gage positions again were approximately 5-, 10-, and 15-mm from the impact surface of the specimen. The induction wire gages were fabricated from 0.0015-in. copper wire. A schematic of the particle velocity gage method is shown in Figure 7. The inductor length, parallel to the magnetic pole faces, was 0.25 or 0.6 in. depending upon whether mixture 6A or mixture 75A, respectively, was the specimen material. A pair of particle velocity gages was placed at each of the measurement positions in shot 1094. This was done to determine the variation in the wave profiles caused by the large aggregate in mixture 75A after propagation through the same distance. The induction wire leads were all brought out to the edge of the specimen then to the back in a manner similar to technique 2 (Figure 21) as described for manganin gages. Care was taken to keep the leads parallel to each other and normal to the magnetic field. No problem was encountered in gage loss due to lead failure primarily because the current flow was very low as compared to the manganin gages, eliminating hot spot burnout.

59. Data analysis for all particle velocity gaged shots was accomplished using the method noted earlier in Part III. Only one of 18 particle velocity gages failed during test in this study.

60. The stress reflection method described earlier was used in shot 1091 on mixture 75A. This method is dependent only upon the impedance mismatch between the witness and specimen materials. As developed to date this method does not account for multiple wave behavior. Consequently, shot 1091 was conducted in part for comparison with the results of the other methods since multiple wave behavior was observed for mixture 75A. A manganin foil gage as described earlier in this section was sandwiched between two 3-mm thick Plexiglas disks. A disk of mixture 75A was bonded to one of the Plexiglas surfaces. Another manganin gage was sandwiched within the 75A disk to measure the "in-material" stress for comparison with the first gage. Gage lead configuration was that of lead technique 2 (Figure 21).

PART VII: DISCUSSION OF RESULTS

Verification of Computer Modeling

61. The primary objective of the computer study was to simulate the shock response of mixture 75A concrete so that the results could be used in experimental design. It was apparent that the success of this simulation was dependent upon (a) the successful shock response modeling of the primary constituents--Wyoming granite aggregate and the cement matrix, and (b) a satisfactory physical model of the mixture.

Shock response modeling of primary constituents

62. Since no experimental data were available upon which to base the desired response of the concrete matrix of mixture 75A, the response of mixture 6A was used with modifications as noted in Part V. Computer simulated and experimental stress-time profiles of mixture 6A are shown in Figure 22. It is readily apparent that the waveforms are different. The experimental stress-time profiles show a much faster rise time relaxation than do the computer simulated waveforms. This is due in part to the porosity (= 20 percent) of concrete mixture 6A. The computer code does not adequately model this porous material behavior. Greater accuracy may be obtained by varying the artificial viscosity coefficients in the code; however, this was not attempted.

63. A comparison of results that has more meaning is the Hugoniot stress-particle velocity curves shown in Figure 23 determined from simulated and experimental data for mixture 6A and the simulated data for the

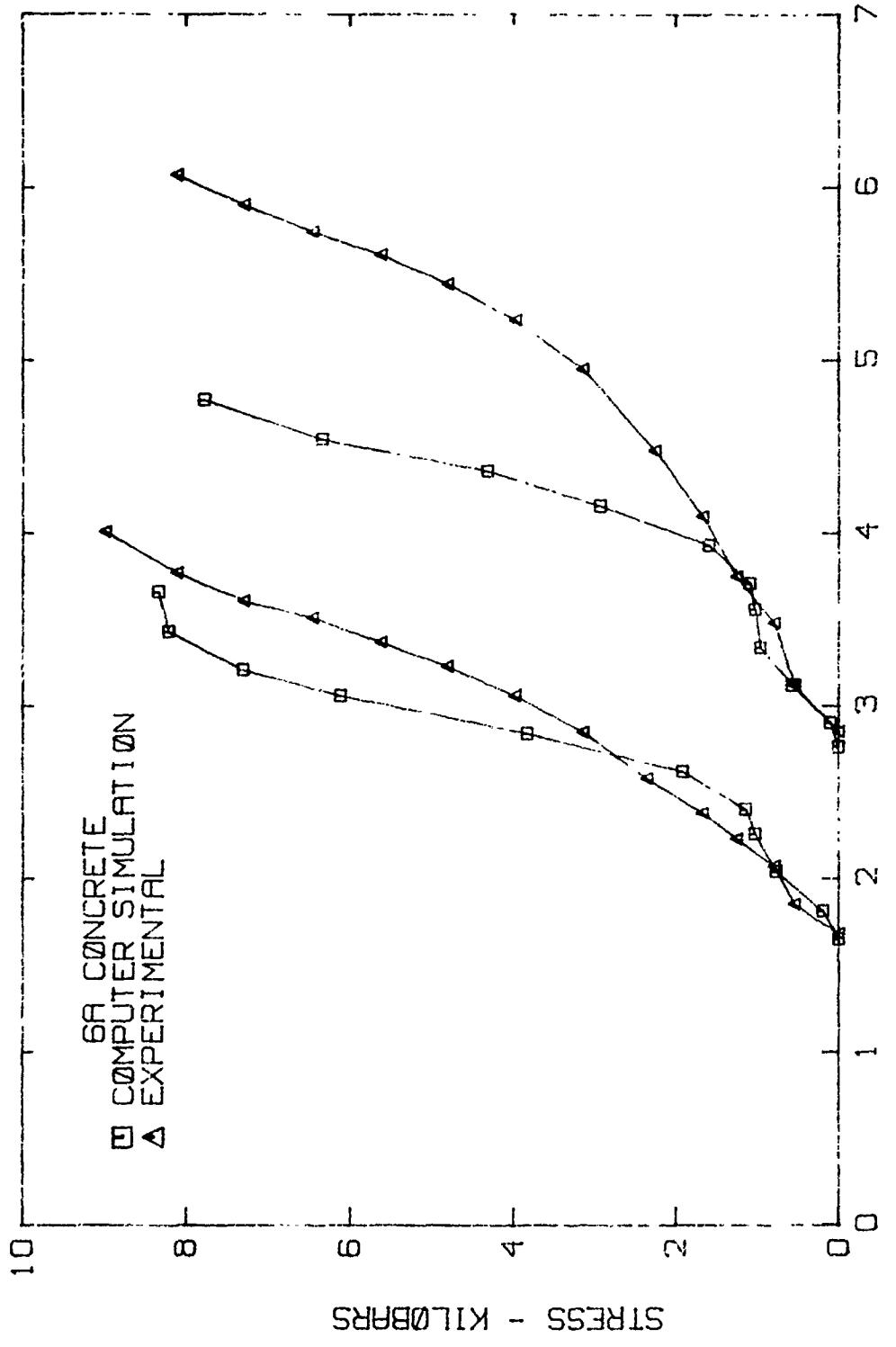

Figure 22. Computer simulated and experimental stress-time profiles for 6A concrete

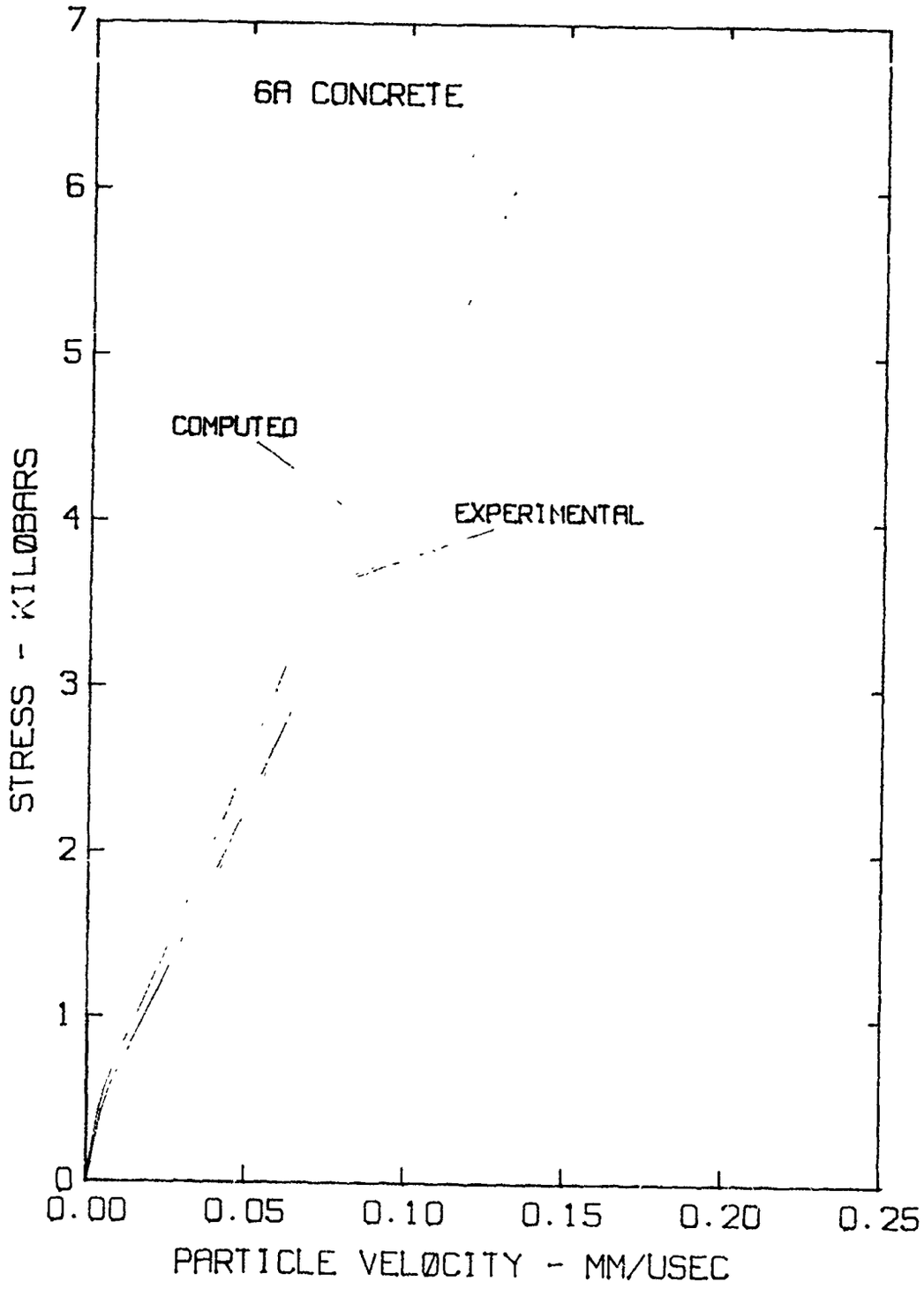

Figure 23. Computer simulated and experimental stress-particle velocity Hugoniots for 6A concrete

cement matrix material. These show the modeling to be close for mixture 6A and about as estimated for the matrix material. The matrix material could be expected to have a lower slope when compared with the simulated results of mixture 6A because of lower density ($\approx$ 3 g/cc less) for the matrix material. It is evident then that the general profile shape, in this case a ramped double-step front, rather than an exact mirror image profile of stress versus time is the controlling factor in the Hugoniot curves provided that average incremental shock velocities between profiles are closely matched. This is the case in the comparison just described.

64. As noted earlier in Part V, difficulty was encountered in obtaining a mathematically stable computer calculation and at the same time properly modeling the granite. Figure 24 illustrates a comparison between stress-time profiles from computer run 3 and experimental profiles obtained for the granite in another study. The computer profiles show a faster relaxing shock front with time and greater curvature near peak stress. The difference obtained is thought to be due in part to the result of the computer code spreading the front over several calculation meshes in the model. Figure 25 shows the Hugoniot stress-particle velocity curves determined from simulated and experimental data for the granite. Figure 24 shows the computer modeling accuracy to be within acceptable limits.

65. Because of the above comparisons it is evident that the computer shock response modeling of the constituent materials of mixture 75A was successful.

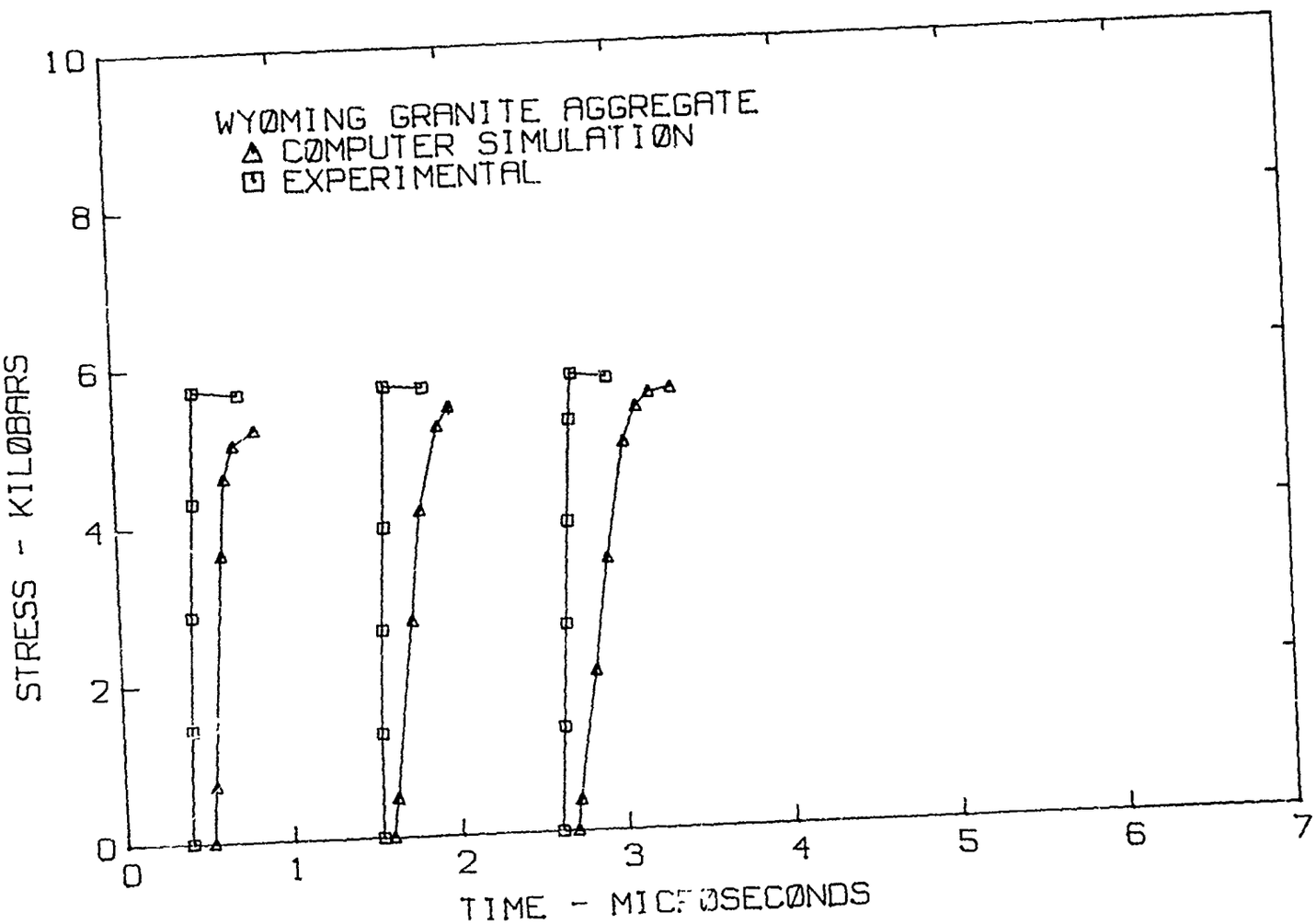

Figure 24. Computer simulated and experimental stress-time profiles for Wyoming granite

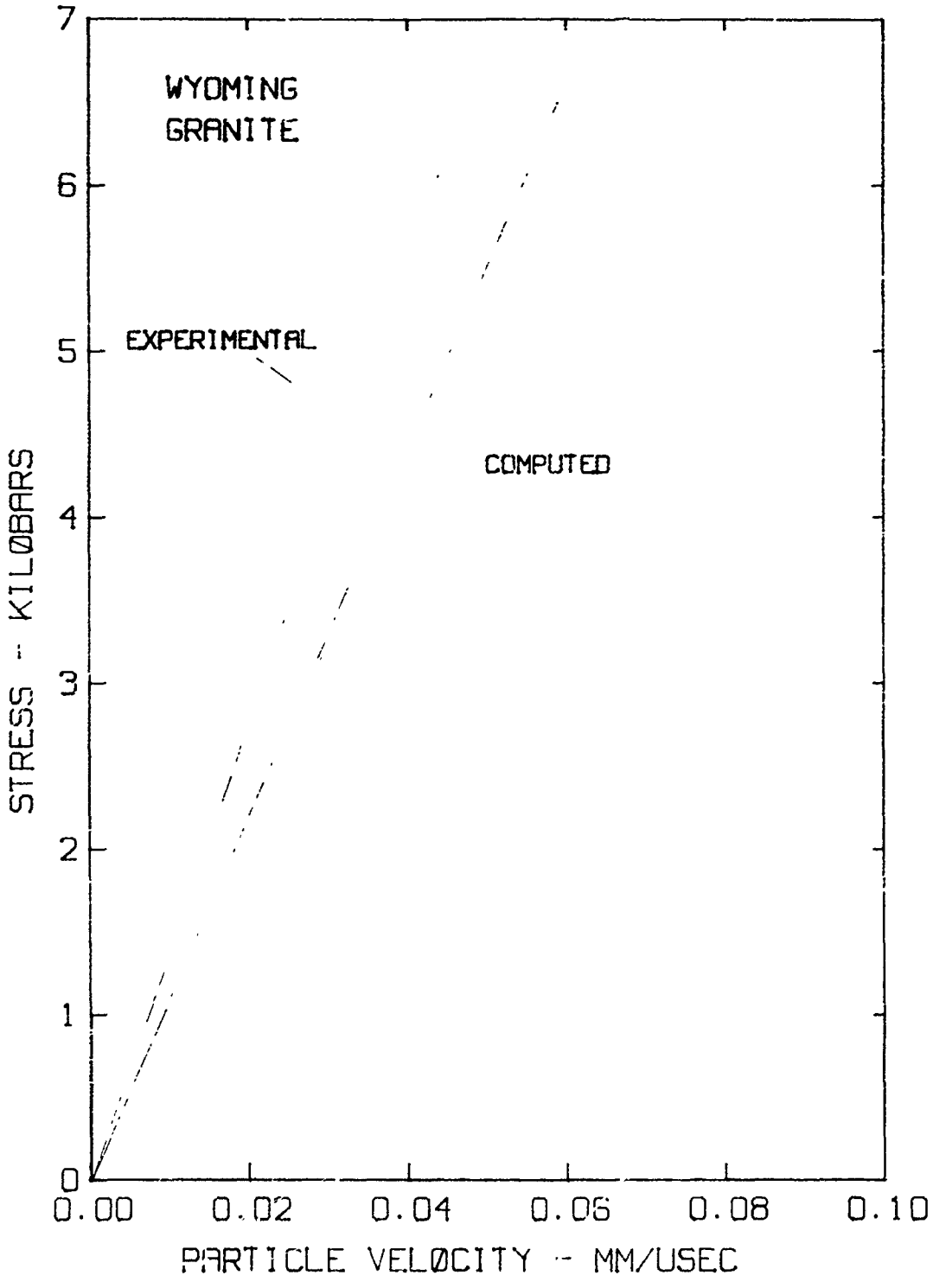

Figure 25. Computer simulated and experimental stress-particle velocity Hugoniots for Wyoming granite

Verification of the physical model

66. The averaged stress-time profiles of computer runs 4 and 5 at i = 16, 30, 44, and 58 (lines I-IV, Figures 13-14) in Figure 18, described in Part V, should be compared. The profiles at each of the positions along the propagation path are virtually identical with the exception of the profile at i = 44 (line III). The aggregate position was different along this line as noted in Figures 13 and 14. The proportion of aggregate and matrix encountered along this line was different. When the line at i = 44 in run 5 was shifted from j = 2-15 to j = 6-19, to encompass the same proportion of constituents, the averaged stress-time profiles became identical between runs 4 and 5. This indicated that the gage position was very important when constructing an experimental specimen at least for the case where the maximum particle size is one-third of the gage size. Consequently, during specimen construction stress and particle velocity gages were placed in a manner that encompassed the same proportion of aggregate and matrix material. This proportion was held constant at 43 percent aggregate and 57 percent matrix. This procedure eliminated the error described above at least to the extent that surface aggregate position could be determined. It should be noted that even though the aggregates at i = 44 were positioned differently in runs 4 and 5, the profiles at i = 58 did not change. Therefore, aggregate orientation in the model does not affect the results as long as the aggregate is equally spaced throughout the model.

67. In order to complete the evaluation of the computer modeling of mixture 75A, comparisons must be made with experimental data. Figures 26 and 27 show stress and particle velocity versus time wave profiles for computer run 4 and experimental shots 1092 and 1095. The stress levels of the two shots were higher than the peak stresses in the model; however, the wave profiles are generally similar. Although there is a great deal more time-spreading of the experimental wavefronts, as was seen earlier in Figure 22 for mixture 6A, the profile shapes are comparable. Both experimental and computer data show that the peak stress and particle velocity profiles attenuate with increased propagation distance.

68. A final comparison is made in Figure 28 where Hugoniot stress-particle velocity relationships are shown for experimental and computer data on 75A concrete. The experimental curve was determined as a best fit through all mixture 75A data. The computer simulated curve was obtained from a best fit of the results of runs 4 and 5. Within the range of stresses shown, the stress-particle velocity Hugoniots compare very well. These data indicate that the constituent material modeling and the physical layout model of the constituents were acceptable. It was determined that the results of the computer studies could be used with confidence to assist in experimental specimen design and serve as an aid in experimental analysis.

Evaluation of Experimental Data

69. The EOS tests on mixture 6A fell within the range of values determined by General Motors[30] (GM) shown in Figure 29. The slope of

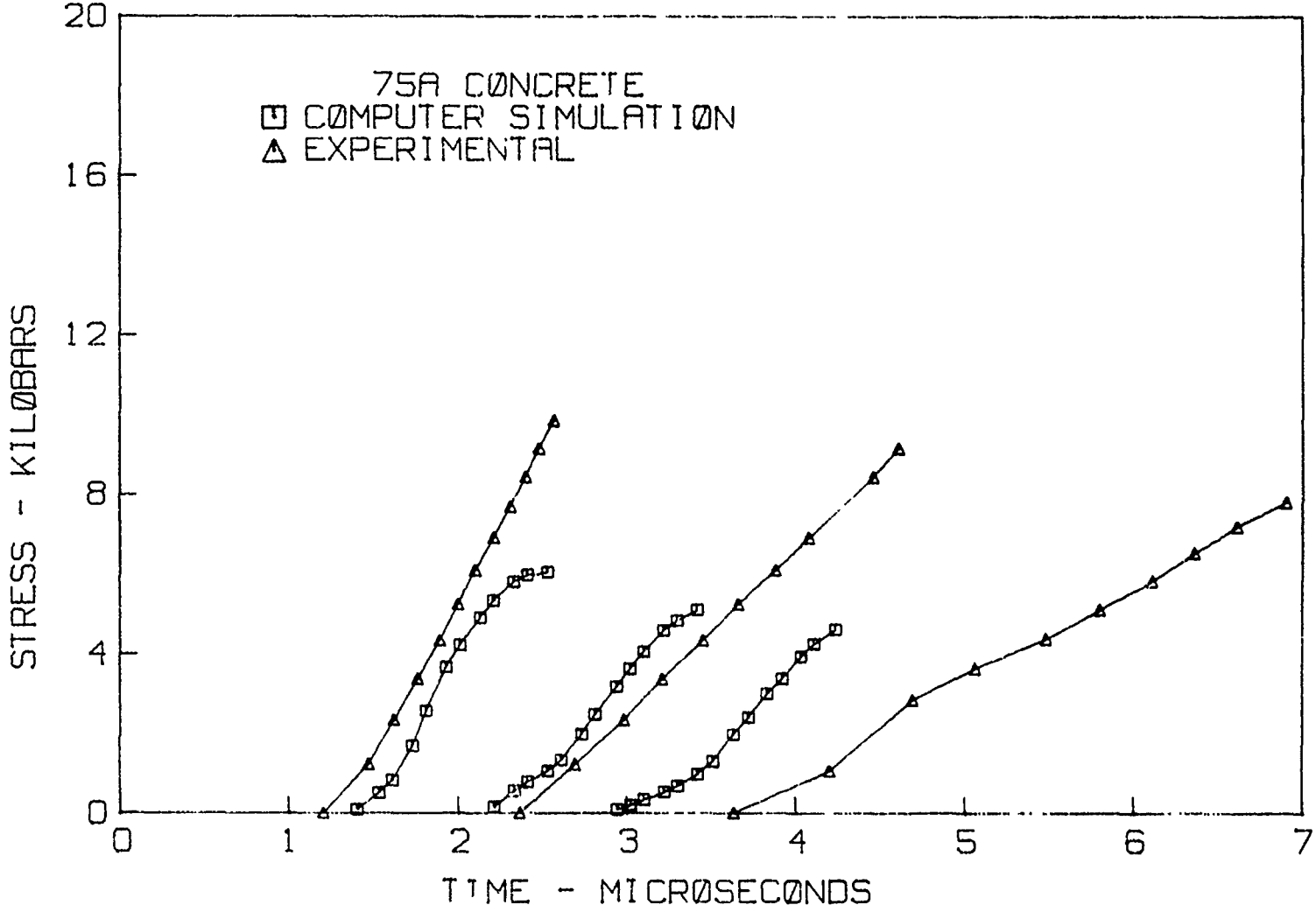

Figure 26. Computer simulated and experimental stress-time profiles for 75A concrete

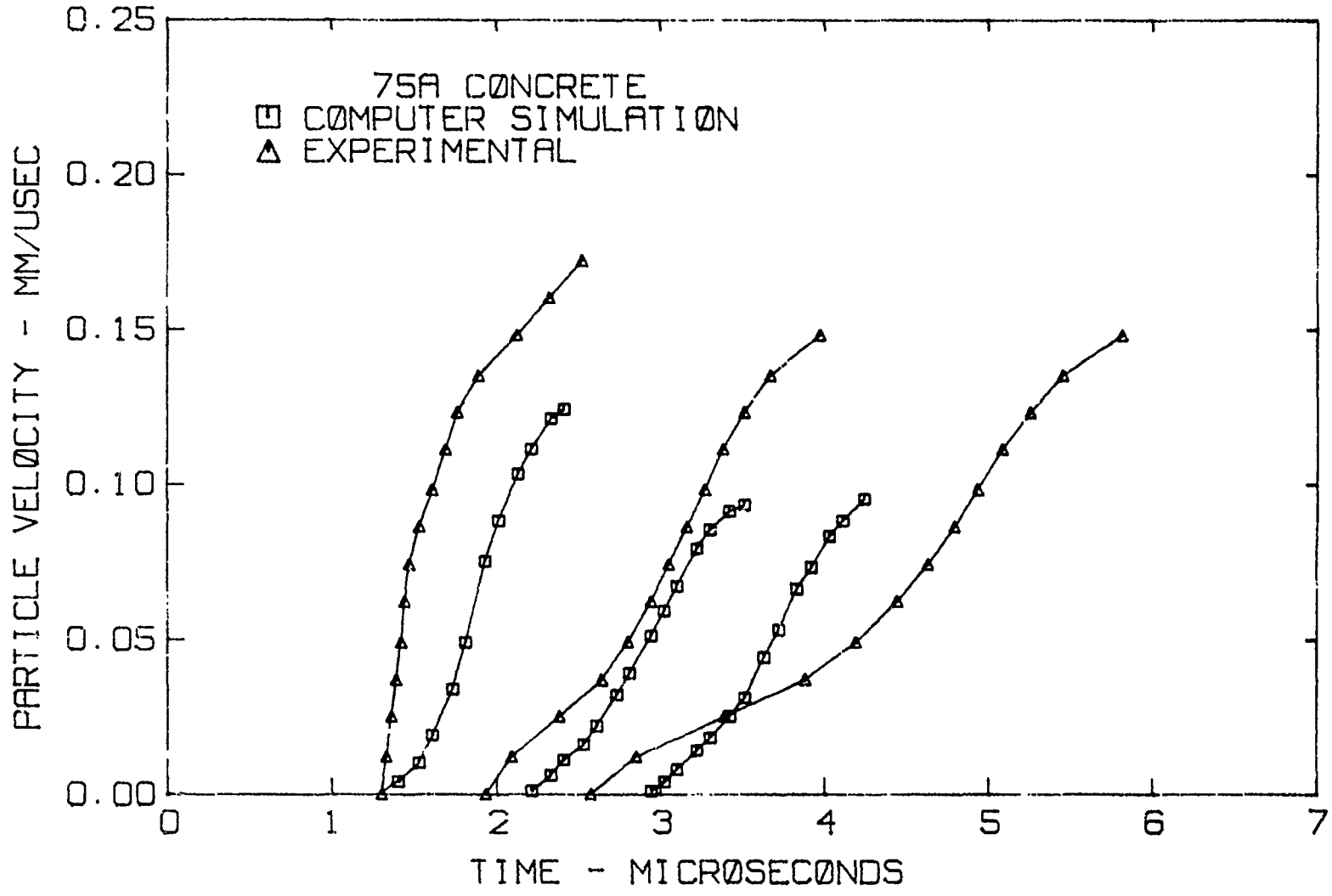

Figure 27. Computer simulated and experimental particle velocity-time profiles for 75A concrete

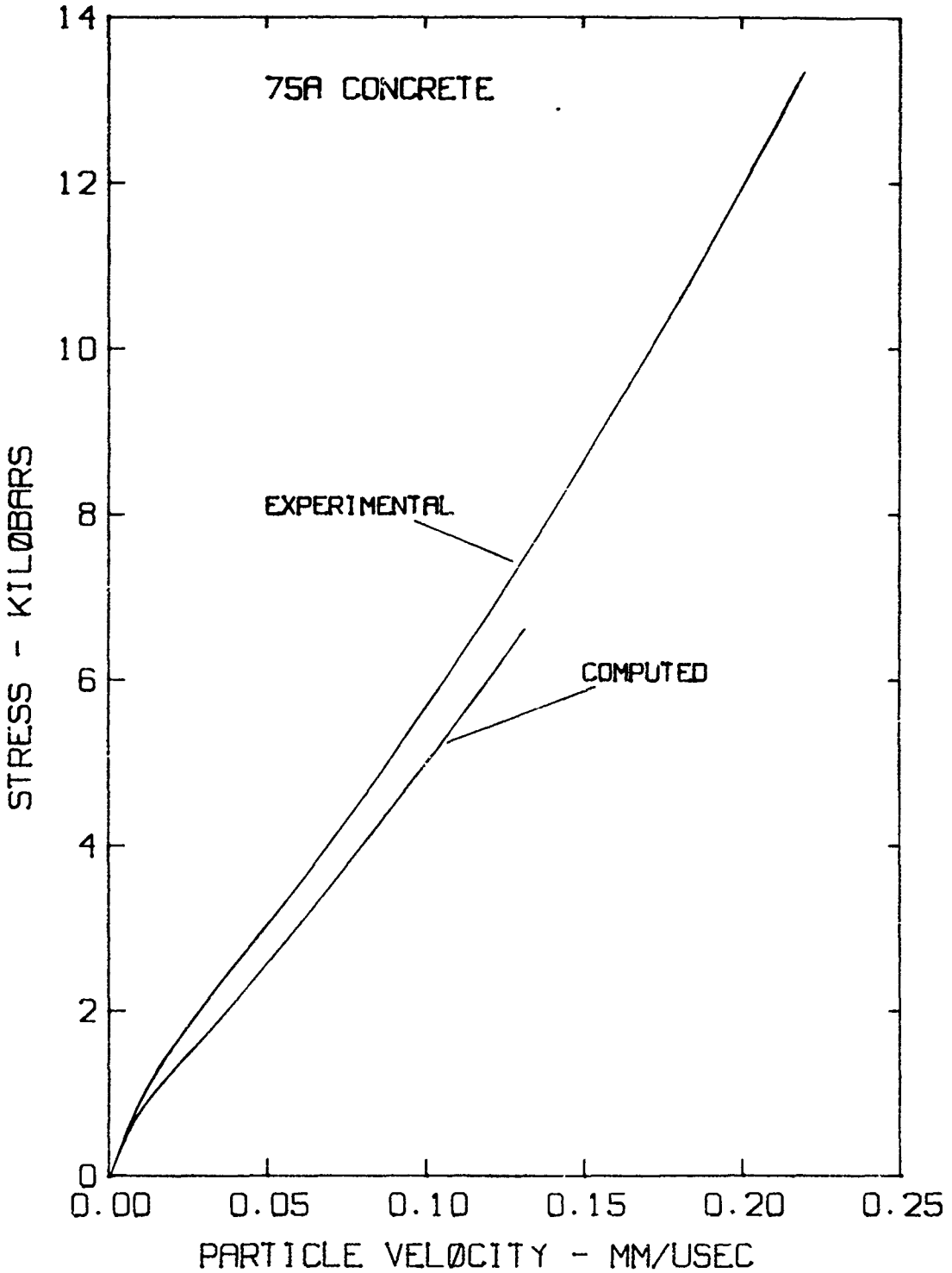

Figure 28. Computer simulated and experimental stress-particle velocity Hugoniots for 75A concrete

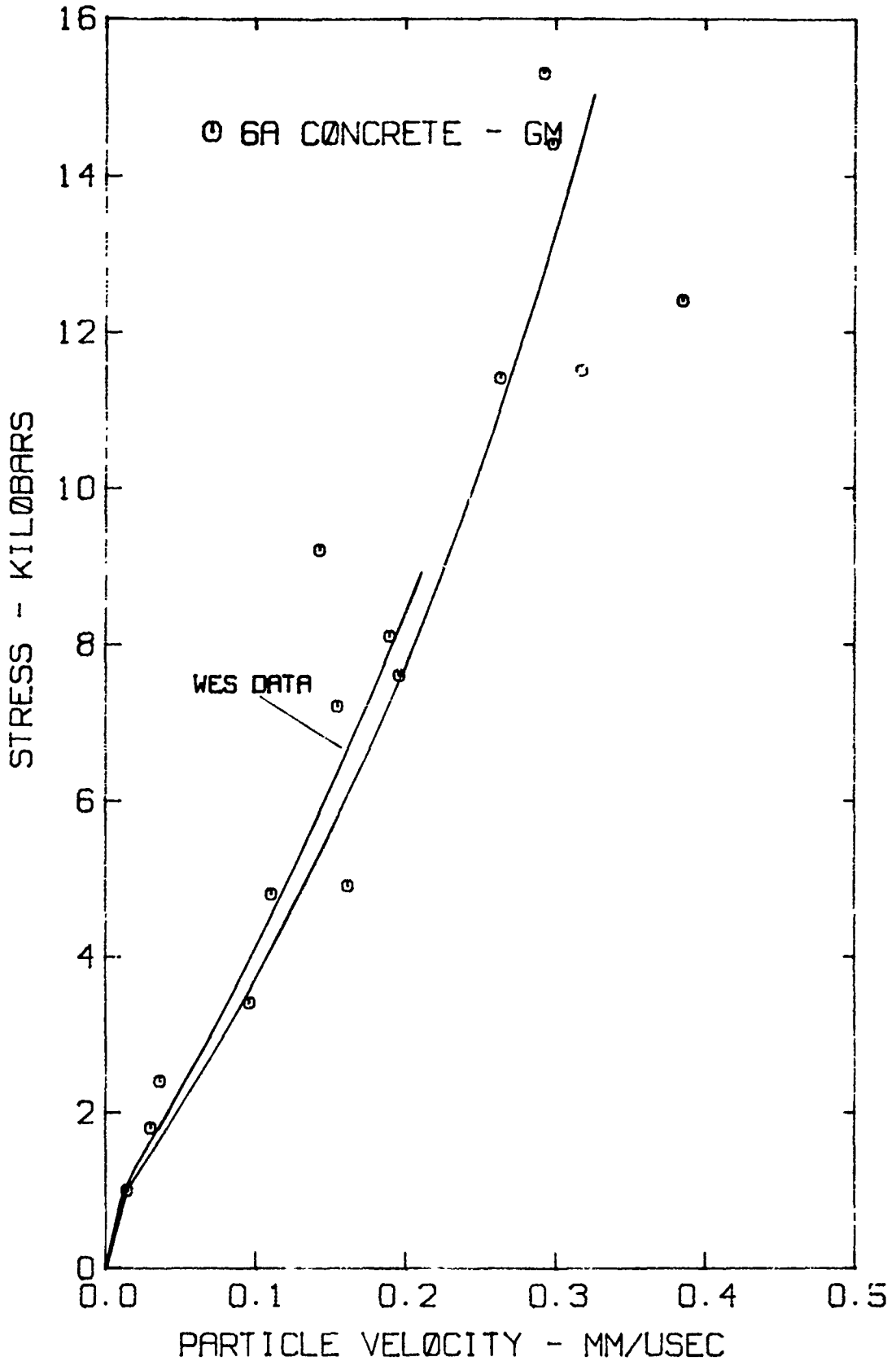

Figure 29. WES and GM stress-particle velocity Hugoniots for 6A concrete

the Hugoniot for these tests was based upon a best fit of data points and was slightly higher than the GM best fit line. The difference can be attributed to the methods of data analysis used. The incremental analysis of nonideally shaped multiple-front shock waves used in this study generally produces slightly higher sloped Hugoniot curves.

70. The data produced from the EOS tests of mixture 75A did show considerable scatter; however, the error was within acceptable limits. It was noted in the analysis of each set of three gages per test that the profiles varied considerably from test to test in the initial 10 mm of propagation distance within the specimen. It was also noted that calculations involving the first gage located $\approx$ 5 mm from the impact surface produced the greatest experimental error. Shot 1094, in which a pair of gages was located at each measurement depth, showed that the wave profile of each pair of gages became increasingly similar with increasing propagation distance. In this test the third pair of gages located 15 mm into the specimen produced identical profiles. These observations indicated that at least one matrix-aggregate interface must be encountered between the stress input surface and the first measurement point. It also appears that the first gage should be located at a minimum distance of 1.5 times the mean coarse aggregate size from the impact surface. It also can be inferred that the minimum distance between gages should not be less than one-half of the mean coarse aggregate size. The accepted distance-particle size relationship normally desired is 10:1. The relationships proposed here should produce a slightly greater but still acceptable error.

71. Measurement error is also a function of the gage size. Although the 0.25-in.-square manganin gages and the 0.6-in.-long particle velocity gages used in this study produced usable data, it is felt that the size of gages used when conducting EOS tests of concrete should be equal to or greater than the maximum aggregate size. The use of larger gages accurately placed to be in contact with the same proportion of constituent materials as exist by volume in the concrete mixture will enhance the reproducibility of results. This was verified by analysis of the computer study results.

72. The results calculated from shot 1091 using the stress reflection method fell within the range of data produced by the other methods. In this test the "in-material" gage failed before peak stress was reached. The reflection gage in Plexiglas successfully recorded long after the reflected stress wave was observed; thus, the Hugoniot state for the shot was determined from the reflection gage. The question arising from use of the stress reflection method in a zone of known multiple wave response was not resolved. It would appear that the method is acceptable for determination of the final state when multiple wave response occurs, but that intermediate states will not be determined.

73. The best fit experimental Hugoniot curves for 6A and 75A concrete shown in Figures 19 and 20 indicate that mixture 6A was a relatively close match for 75A concrete. In all probability if the water content in mixture 6A had been reduced somewhat, the match would have been nearly exact. At the time that mixture 6A was prepared, difficulty was encountered in removing large entrapped air voids. Consequently, the

water-cement ratio was increased slightly to aid in vibration of the fresh concrete. The additional water contributed to an increase in the air dry porosity of mixture 6A effectively reducing the slope of the Hugoniot curves. Vibratory techniques recently developed at WES have allowed good consolidation of the mixture at greatly reduced water content. It is felt that mixture 6A could now be altered by reduced water content to exactly match the Hugoniot of mixture 75A. Although the conclusions reached here regarding the Hugoniot match between mixtures 6A and 75A only have verification in the stress range 0-10 kilobars, it is felt that the EOS match at higher stress levels would be comparable.

PART VIII: CONCLUSIONS AND RECOMMENDATIONS

74. Based upon the results obtained in this study, the following conclusions are made.

a. The Hugoniot equation of state of a standard structural concrete having maximum aggregate size of $\leq$ 1 in. can be determined within reasonable limits of experimental error.

b. A modeled concrete having a maximum aggregate size of $\leq$ 1/8 in. can be designed to match the EOS of the prototype sized aggregate concrete. The design of the modeled mixture should be based upon the use of identical proportions of constituent materials. The EOS match is also dependent upon closely matching the porosity, longitudinal sound speed, and unconfined compressive strength.

c. The placement of "in-material" gages in a prototype aggregate concrete is critical especially if the gage size is less than or equal to the maximum aggregate size. Each gage should encompass the same proportion of constituents by volume as in the prototype concrete mixture.

d. The minimum distances between the shock wave input boundary and the first gage position and the distances between gages were determined to be 1.5 and 0.5 times the mean coarse aggregate size, respectively.

e. TOODY I, a two-dimensional wave propagation computer code, was found to calculate the EOS properties of a composite aggregate-concrete matrix model with no greater error than that obtained by the EOS modeling of the constituent components.

f. The computer code results do aid in the design of test specimen and the analysis of experimental data.

g. The stress reflection method is well adapted to EOS determinations for concrete, especially at stress levels that produce single wave behavior. The only requirement of the stress input method is that the shock pulse is flat-topped.

75. Based upon the work done and conclusions reached in this study, the following recommendations are made.

a. EOS experiments on prototype sized aggregate concretes require an input plane wave size of at least 2-in. diameter and preferably 4-in. diameter because of the larger than standard total sample depth required to properly measure EOS parameters.

b. Because of the larger specimen size requirement it is recommended that EOS tests conducted with flat-plate gun impact the projectile be designed to ensure that the specimen will not be unloaded prior to complete measurement of the loading phase. This means that the projectile impact disk length must be long enough to ensure a long, flat-topped shock pulse. The length of the pulse is based upon the differences between the shock loading and unloading wave velocities.

c. When using the direct-contact explosives method it is recommended that the driver explosive be long enough to produce a flat-topped shock pulse throughout the total measurement depth.

d. In order to produce the same input pulse width with the flyer-plate explosive system it is recommended that the flyer plate have adequate thickness to ensure a long, flat-topped shock pulse.

e. The stress range produced by explosives systems should provide single wave hydrodynamic behavior in concrete. Unless a phase change takes place (GM suspected one at $\approx$ 120 kilobars in mixture 6A), measurement methods such as time of arrival pins or the stress reflection method using manganin gages would provide adequate measurement accuracy. When using time of arrival pins it is recommended that a sufficient number be used to ensure accurate measurement of propagation velocity. Also, that the specimen distance through which these measurements are made is representative of the composite material.

f. If phase changes are suspected, time of arrival pins should be supplemented by a manganin gage to determine if a multiple wave shock front exists. The gage will aid in the determination of the propagation velocities of each wave.

g. The stress reflection method does not rely upon shock wave propagation through the specimen material. Therefore, it is recommended that this method be used when difficulty is encountered in obtaining a long input shock pulse.

h. It is also recommended that additional work be conducted with the stress reflection method to better understand its use in zones of multiple-wave behavior.

1. "Cement and Concrete Terminology," American Concrete Institute Special Publication SP-19, 1967.

2. Rice, M. H., Walsh, J. M., and McQueen, R. G., "Compression of Solids by Strong Shock Waves," Solid State Physics, Vol 6, 1958, edited by F. Seitz and D. Turnbull, Academic Press Inc., New York, pp 1-63.

3. Ahrens, T. J., Rosenberg, J. T., and Ruderman, M. H., "Dynamic Properties of Rock," DASA 1869, 30 Sep 1966, Stanford Research Institute, Menlo Park, California.

4. Anderson, G. D., et al., "Stress Relaxation in the Shock Compression of Solids," Air Force Weapons Laboratory Technical Report No. AFWL-TR-67-24, May 1967, Stanford Research Institute, Menlo Park, California.

5. Erkman, J. O., "Hydrodynamic Theory and High Pressure Flow in Solids," DASA 1397, 15 July 1963, Stanford Research Institute, Menlo Park, California.

6. Ainsworth, D. L., "New Applications of Grout and Concrete as Shock Impedance Matching Materials for Geologic Formations," Miscellaneous Paper No. C-72-10, April 1972, U. S. Army Engineer Waterways Experiment Station, CE, Vicksburg, Mississippi.

7. Jones, A. H., Isbell, W. M., and Maiden, C. J., "Measurement of the Very-High-Pressure Properties of Materials Using a Light-Gas Gun," TR 65-84, Nov 1965, GM Defense Research Laboratories, Santa Barbara, California.

8. Fowles, G. R., et al., "Gas Gun for Impact Studies," The Review of Scientific Instruments, Vol 41, No. 7, July 1970. pp 984-996.

9. Minshall, S., "Properties of Elastic and Plastic Waves Determined by Pin Contactors and Crystals," Journal of Applied Physics, vol 20, No. 4, April 1955, pp 463-469.

10. Sugiuchi, H., "Determination of the Hugoniot Equation of State of Grout, Report 1, 1963 Tests," Technical Report No. 6-669, Jan 1965, U. S. Army Engineer Waterways Experiment Station, CE, Vicksburg, Mississippi.

11. Dremin, A. N., and Adadurov, G. A., "Behavior of Glass under Dynamic Loading," Soviet Physics Solid State, Vol 6, 1964, pp 1379-1384.

12. Dremin, A. N., Pershin, S. V., and Pogorelov, V. F., "Structure of Shock Waves in KCl and KBr Under Dynamic Compression to 200,000 Atm," Combustion, Explosion, and Shock Waves, Vol 1, 1965, pp 1-4.

13 Ainsworth, D. L., and Sullivan, B. R., "Shock Response of Rock at Pressures Below 30 Kilobars," Technical Report No. 6-802, Nov 1967, U. S. Army Engineer Waterways Experiment Station, CE, Vicksburg, Mississippi.

14. Murri, W. J., and Smith, C. W., "Equation of State of Rock," Interim Technical Report, 31 Mar 1970, Stanford Research Institute, Menlo Park, California.

15. Sullivan, B. R., Ainsworth, D. L., and Bombich, A. A., "Technique for Determining Unloading Response of Rock," Miscellaneous Paper C-74-6, April 1974, U. S. Army Engineer Waterways Experiment Station, CE, Vicksburg, Mississippi.

16. Foules, G. R., "Determination of Constitutive Relations from Plane Wave Experiments," Paper presented at Western Applied Mechanics Conference, 25 Aug 1969, Albuquerque, New Mexico.

17. Keough, D. D., "Procedure for Fabrication and Operation of Manganin Shock Pressure Gages," Air Force Weapons Laboratory, Technical Report No. AFWL-TR-68-57, Aug 1968, Stanford Research Institute, Menlo Park, California.

18. Keough, D. D., "Pressure Transducer for Measuring Shock Wave Profiles Phase IX: Additional Gage Development," DASA 1414-1, Final Report, Nov 1964, Stanford Research Institute, Menlo Park, California.

19. Keough, D. D., "Development of a High-Sensitivity Piezoresistive Shock Transducer for the Low Kilobar Range," DASA 2508, Final Report, 25 March 1970, Stanford Research Institute, Menlo Park, California.

20. Ginsberg, M. J., "Calibration and Characterization of Ytterbium Stress Transducers," DNA 2742F Final Report--Task III, October 1971, Stanford Research Institute, Menlo Park, California.

21. Rice, M. H., "Calibration of the Power Supply for Manganin Pressure Gages," Air Force Weapons Laboratory Technical Report No. AFWL-TR-70-120, Nov 1970, Air Force Weapons Laboratory, Kirtland Air Force Base, New Mexico.

22. Froula, N., "Hugoniot Equation of State and Stress Wave Propagation in Saturated Ottawa Banding Sand at +20 and -10 Degree Centigrade," Sep 1971, Systems, Science, and Software, La Jolla, California.

23. "Material Property Investigation for ESSEX I Test Site at Fort Polk," U. S. Army Engineer Waterways Experiment Station Report to be published.

24. Froula, N. H., Suenaga, E. L., and Bryson, R. L., "Shock Compression and Release Behavior of Two Nevada Test Site Tuffs," DNA 2851F Final Report, July 1972, Systems, Science, and Software, La Jolla, California.

25. Bembich, A. A., and Sullivan, B. R., "Development of Hugoniot Equation of State Media Matching Grout for ESSEX I at Fort Polk," U. S. Army Engineer Waterways Experiment Station Report to be published.

26. Fowles, G. R., "Shock Compression of Quartz," Ph.D. thesis, 1961, Department of Geophysics, Stanford University.

27. Eden, G., and Wright, P. W., "A Technique for the Precise Measurement of the Motion of a Plane Free Surface," Proceedings Fourth Symposium (International) on Detonation, Office of Naval Research, ACR-126, 1965, pp 573-583.

28. Barker, L. M., "Laser Interferometry in Shock-Wave Research," Experimental Mechanics, May 1972, pp 209-215.

29. Ingram, G. E., and Graham, R. A., "Quartz Gauge Technique for Impact Experiments," Proceedings Fifth Symposium (International) on Detonation, Office of Naval Research, ONR Report DR-163, 1970, pp 294-312.

30. Gregson, V. G., Jr., "A Shock Wave Study of Fondu-Fyre WA-1 and a Concrete," DNA 2797F, Feb 1972, General Motors Materials and Structures Laboratory, Warren, Michigan.

31. Sullivan, B. R., "Dynamic Compaction of Porous Concrete," Miscellaneous Paper C-68-9, Nov 1968, U. S. Army Engineer Waterways Experiment Station, CE, Vicksburg, Mississippi.

32. Thorne, B. J., and Herrman, W., "TOODY--A Computer Program for Calculating Problems of Motion in Two Dimensions," SC-RR-66-602, July 1967, Sandia Laboratories, Albuquerque, New Mexico.

33. Stowe, R. L., "Development of a Deformational Apparatus in Conjunction with Constitutive Property Tests--Project DIDO QUEEN," U. S. Army Engineer Waterways Experiment Station Report to be published.

34. Keough, D. D., and Williams, R. F., "Piezoresistive Transducer for Shock Wave Studies," Air Force Weapons Laboratory Technical Report No. AFWL-TR-67-81, Dec 1967, Stanford Research Institute, Menlo Park, California.